

# Forest-atmosphere exchange of reactive nitrogen in a **low-polluted remote region area** – Part I: Measuring temporal dynamics

Pascal Wintjen<sup>1</sup>, Frederik Schrader<sup>1</sup>, Martijn Schaap<sup>2,3</sup>, Burkhard Beudert<sup>4</sup>, and Christian Brümmer<sup>1</sup>

<sup>1</sup>Thünen Institute of Climate-Smart Agriculture, Bundesallee 68, 38116, Braunschweig, Germany

<sup>2</sup>TNO, Climate Air and Sustainability, Utrecht, 3584 CB, The Netherlands

<sup>3</sup>Institute of Meteorology, Freie Universität Berlin, 12165 Berlin, Germany

<sup>4</sup>Bavarian Forest National Park, 94481, Grafenau, Germany

**Correspondence:** Pascal Wintjen (pascal.wintjen@thuenen.de)

**Abstract.** Long-term dry deposition flux measurements of reactive nitrogen based on the eddy-covariance or the aerodynamic gradient method are scarce. Due to the large diversity of reactive nitrogen compounds and high technical requirements for the measuring devices, simultaneous measurements of individual reactive nitrogen compounds are not affordable. Hence, we examined the exchange patterns of total reactive nitrogen ( $\Sigma N_r$ ) and determined annual dry deposition budgets based on measured data at a **low-polluted** mixed forest **exposed to low air pollution levels** located in the Bavarian Forest National Park (NPBW), Germany. Flux measurements of  $\Sigma N_r$  were carried out with a Total Reactive Atmospheric Nitrogen Converter (TRANC) coupled to a chemiluminescence detector (CLD) for 2.5 years.

The average  $\Sigma N_r$  concentration was  $3.1 \mu\text{g N m}^{-3}$ . Denuder measurements with DELTA samplers and chemiluminescence measurements of nitrogen oxides ( $\text{NO}_x$ ) have shown that  $\text{NO}_x$  has the highest contribution to  $\Sigma N_r$  ( $\sim 51.4\%$ ), followed by ammonia ( $\text{NH}_3$ ) ( $\sim 20.0\%$ ), ammonium ( $\text{NH}_4^+$ ) ( $\sim 15.3\%$ ), nitrate  $\text{NO}_3^-$  ( $\sim 7.0\%$ ), and nitric acid ( $\text{HNO}_3$ ) ( $\sim 6.3\%$ ). Only slight seasonal changes were found in the  $\Sigma N_r$  concentration level whereas a seasonal pattern was observed for the contribution of  $\text{NH}_3$  and  $\text{NO}_x$ .  $\text{NH}_3$  showed highest contributions to  $\Sigma N_r$  in spring and summer,  $\text{NO}_x$  in autumn and winter.

We observed deposition fluxes at the measurement site with median fluxes ranging from  $-15$  to  $-5 \text{ ng N m}^{-2} \text{ s}^{-1}$  (negative fluxes indicate deposition). Median deposition velocities ranged from  $0.2$  to  $0.5 \text{ cm s}^{-1}$ . In general, highest deposition velocities were recorded during high **incident solar** radiation, in particular from May to September. Our results suggest that seasonal changes in composition of  $\Sigma N_r$ , global radiation ( $R_g$ ) and other drivers correlated with  $R_g$  were most likely influencing the deposition velocity ( $v_d$ ). We found that from May to September higher temperatures, lower relative humidity, and dry leaf surfaces increase  $v_d$  of  $\Sigma N_r$ . At the measurement site,  $\Sigma N_r$  concentration did not emerge as a driver for the  $\Sigma N_r v_d$ .

No significant influence of temperature, humidity, friction velocity, or wind speed on  $\Sigma N_r$  ~~dry deposition sums were~~ fluxes when using the Mean-Diurnal-Variation (MDV) approach for filling gaps of up to five days was found. ~~We used the Mean-Diurnal-Variation (MDV) approach for filling gaps of up to five days.~~ Remaining gaps were replaced by a monthly average of the specific half-hourly value. From June 2016 to May 2017 and June 2017 to May 2018, we estimated dry deposition sums of  $3.8$  and  $4.0 \text{ kg N ha}^{-1} \text{ a}^{-1}$ , respectively. Adding results from the wet deposition measurements, we determined  $12.2$  and  $10.9 \text{ kg N ha}^{-1} \text{ a}^{-1}$  as total nitrogen deposition in the two years of observation.

25 This work encompasses (one of) the first long-term flux measurements of  $\Sigma N_r$  using novel measurements techniques for estimating annual nitrogen dry deposition of to a remote forest ecosystem.

## 1 Introduction

Reactive nitrogen ( $N_r$ ) compounds are essential nutrients for plants. However, an intensive supply of nitrogen by fertilisation or atmospheric deposition is harmful for natural ecosystems and leads to a loss of biodiversity through soil acidification and eutrophication (Krupa, 2003; Galloway et al., 2003) and may also threaten human health by acting as precursors for ozone ( $O_3$ ) and  $PM_{2.5}$  (Erisman et al., 2013). Atmospheric nitrogen load increased significantly during the last century due to intensive crop production and livestock farming (Sutton et al., 2011; Flechard et al., 2011, 2013; Sutton et al., 2013) (mainly through ammonia) and fossil fuel combustion by traffic and industry (mainly through nitrogen dioxide and nitric oxide). The additional amount of  $N_r$  enhances biosphere-atmosphere exchange of  $N_r$  (Flechard et al., 2011), affects plant health (Sutton et al., 2011) and influences the carbon sequestration of ecosystems such as forests (Magnani et al., 2007; Högberg, 2007; Sutton et al., 2008; Flechard et al., 2020), although the impact of increasing nitrogen deposition on forests carbon sequestration is still under investigation.

For estimating the biosphere-atmosphere exchange of  $N_r$  compounds such as nitrogen dioxide ( $NO_2$ ), nitrogen nitric oxide (NO), ammonia ( $NH_3$ ), nitrous acid (HONO), nitric acid ( $HNO_3$ ) and particulate ammonium ( $NH_4^+$ ) and nitrate ( $NO_3^-$ ), micrometeorological methods such as the eddy-covariance (EC) and the aerodynamic gradient method (AGM) approach have proven their applicability on various ecosystems. The sum of these compounds is called total reactive nitrogen ( $\Sigma N_r$ ) throughout this manuscript. The EC method is the common method for estimating greenhouse gas fluxes (Aubinet et al., 1999; Baldocchi, 2003) in flux monitoring networks (FLUXNET (Baldocchi et al., 2001), ICOS (Heiskanen et al., 2021)) and also suitable for measuring the exchange of  $N_r$  compounds. However, the EC method requires fast-response analyzers. For evaluating fluxes of NO and  $NO_2$  the EC technique has been tested in earlier studies (Delany et al., 1986; Eugster and Hesterberg, 1996; Civerolo and Dickerson, 1998; Li et al., 1997; Rummel et al., 2002; Horii et al., 2004; Stella et al., 2013; Min et al., 2014). In recent years, progress has been made in EC measurements of  $NH_3$  (Famulari et al., 2004; Whitehead et al., 2008; Ferrara et al., 2012; Zöll et al., 2016; Moravek et al., 2019). First attempts in applying EC had been made on  $HNO_3$ , organic nitrogen molecules, nitrate ( $NO_3^-$ ), and ammonium aerosols ( $NH_4^+$ ) (Farmer et al., 2006; Nemitz et al., 2008; Farmer and Cohen, 2008; Farmer et al., 2011). Due to typically low concentrations, high reactivity, and water solubility, measuring fluxes of  $N_r$  compounds is still challenging since instruments need a low detection limit and a response time of  $< 1$  s (Ammann et al., 2012). Thus, fast-response instruments for measuring  $N_r$  compounds like  $HNO_3$  or  $NH_3$  are equipped with a special inlet and short heated tubes to prevent interaction with tube walls (see Farmer et al., 2006; Zöll et al., 2016). However, these instruments need regular maintenance, have a high power consumption, and need a temperature controlled environment for a stable performance. Considering the high technical requirements of these instruments, measuring fluxes of  $HNO_3$  or  $NH_3$  with these instrument is still challenging.

The Total Reactive Atmospheric Nitrogen Converter (TRANC) (Marx et al., 2012) converts all above mentioned  $N_r$  compounds to NO. In combination with a fast-response chemiluminescence detector (CLD), the system allows measurements of  $\Sigma N_r$  with a high sampling frequency. Due to a low detection limit and a response time of about 0.3 s, the TRANC-CLD system can be used for flux calculation based on the eddy-covariance (EC) technique. The key advantage of the TRANC is that only one device is needed for a quantification of the nitrogen dry deposition instead of running several instruments for each compound individually. The TRANC-CLD system has been shown to be suitable for EC measurements above a number of different ecosystems (see Ammann et al., 2012; Brümmer et al., 2013; Zöll et al., 2019; Wintjen et al., 2020).

Only a few long-term studies have been conducted to derive annual inputs with micrometeorological methods at (remote) forest ecosystems. Munger et al. (1996) conducted EC measurements of  $NO_y$ , which refers to the sum of all oxidized  $N_r$  compounds, e.g.,  $NO_2$ , NO,  $HNO_3$ , dinitrogen pentoxide ( $N_2O_5$ ), peroxyacyl nitrates (PAN), aerosol nitrates, above a mixed deciduous forest for five years. Averaged  $NO_x$  concentrations were at 0.62 and 4.26 ppb (0.36 and  $2.44 \mu g N m^{-3}$ ) during summer and winter, respectively, if wind was blowing from Northwest. During southwesterly winds, mean  $NO_x$  concentrations were 1.25 and 9.48 ppb (0.72 and  $5.43 \mu g N m^{-3}$ ) during summer and winter, respectively, indicating a varying pollution climate. The authors reported an annual net dry deposition of  $NO_y$  covering 1990 to 1994 of  $2.49 kg N ha^{-1} a^{-1}$ . Munger et al. (1998) reported an annual reactive N deposition of wet + dry deposition measurements of  $6.4 kg N ha^{-1} a^{-1}$  for the period 1990 to 1996 at the same site. Dry deposition of  $NO_y$  contributed 34% to total deposition. Wet deposition of  $NH_4^+$  was comparatively low estimated to  $1.1 kg N ha^{-1} a^{-1}$ . Neiryneck et al. (2007) and Erisman et al. (1996) conducted AGM measurements in order to estimate dry deposition of  $NO_x$  and  $NH_3$ . Neiryneck et al. (2007) published AGM measurements from July 1999 to November 2001 above mixed coniferous/deciduous forest, which was in close proximity of a highway and the city of Antwerp leading to mean  $NO_2$  and  $NH_3$  concentrations of 8.7 and  $3.0 \mu g N m^{-3}$ , respectively. The authors determined an annual  $NH_3$  dry deposition of  $19.6 kg N ha^{-1} a^{-1}$  and  $NO_x$  emission of  $2.7 kg N ha^{-1} a^{-1}$ .  $NO_x$  emissions were probably related to a strong contribution of soil-emitted NO. Erisman et al. (1996) reported  $NO_x$  and  $NH_3$  fluxes above a Douglas Fir stand of 2.5 ha surrounded by a larger forested area of  $50 km^2$  for 1995. Mean  $NH_3$  concentration was  $4.5 \mu g N m^{-3}$  possibly related to livestock farming in the surroundings of the site. They estimated annual dry depositions of  $17.9 kg N ha^{-1} a^{-1}$  and  $2.8 kg N ha^{-1} a^{-1}$  for  $NH_3$  and  $NO_x$ , respectively. These ~~were the few~~ long-term micrometeorological measurements of  $N_r$  species above forests ~~were made more than 20 years ago and~~ ~~no~~ recent reports on long-term flux measurements of  $N_r$  ~~were found~~ ~~are currently available~~. Since several  $N_r$  compounds contribute to  $\Sigma N_r$  each with different chemical and physical properties, a complex arrangement of different, highly specialized measurement devices would be needed for quantifying  $\Sigma N_r$  exchange. To our knowledge, there is no publication available reporting annual  $\Sigma N_r$  deposition at (remote) forest ecosystems using micrometeorological methods. As stated above, the ~~true outstanding~~ benefit of the TRANC is that the most relevant  $N_r$  species are converted, and a single instrument is sufficient for deriving dry nitrogen deposition. ~~Therewith, we were able to determine annual dry deposition and show seasonal changes in the  $\Sigma N_r$  flux pattern.~~

During a measurement campaign instrumental performance issues and/or periods of insufficient turbulence arise, which require a quality flagging of processed fluxes. Afterwards, the resulting gaps in the measured time-series need to be filled in order to properly estimate long-term deposition budgets. Known gap-filling strategies include the Mean-Diurnal-Variation

(MDV) method, look-up tables (LUT), non-linear regression (NLR) (Falge et al., 2001), marginal distribution sampling (MDS) (Reichstein et al., 2005), and artificial neural networks (Moffat et al., 2007). However, most of these methods have in common that they were originally designed for carbon dioxide (CO<sub>2</sub>) or other inert gases. MDS requires a short-term stability of  
95 fluxes and micrometeorological parameters. This condition is not necessarily fulfilled for  $\Sigma N_r$  and its components. Their exchange patterns are characterized by a higher variability for different time scales leading to a lower autocorrelation and non-stationarities in flux time series compared to inert gases like CO<sub>2</sub>. It is, on the other hand, possible to use statistical methods like MDV or linear interpolation to fill short gaps in flux time series. This was done by Brümmer et al. (2013), but filling long  
100 gaps with this technique is not recommended. Since exchange patterns of  $\Sigma N_r$  can substantially vary each day depending on the composition of  $\Sigma N_r$  and micrometeorology, it is questionable if statistical methods are suitable for  $\Sigma N_r$  considering the high reactivity and chemical properties of its compounds.

Our study is the first one presenting long-term EC flux measurements of  $\Sigma N_r$  above a remote forest. Based on the successful implementation of the TRANC methodology, our objectives are:

1. A discussion of observed concentration and flux patterns of  $\Sigma N_r$  in the context of different temporal scales
- 105 2. An investigation of the influence of micrometeorology on deposition velocities
3. An assessment of annual N deposition using both gap-filling for the dry deposition eddy flux data and complementary wet deposition estimates from local samplers

A follow up paper will investigate the usage of the acquired dataset in a modeling framework to estimate annual N budgets. ~~The study presented here is the first one showing long-term flux measurements of  $\Sigma N_r$  using the EC technique in combination with novel measurement techniques above a remote forest. We discuss the observed flux pattern of  $\Sigma N_r$  (1), show the influence of micrometeorology on deposition velocities (2), and determine dry deposition sums estimated with the MDV approach while considering the influence of micrometeorological parameters (3). Wet deposition results obtained from bulk and wet-only sampler measurements are complementarily used to estimate total deposition. Part II of the paper will present the usage of the acquired dataset in a modeling framework to estimate annual N budgets. Modeled fluxes and deposition velocities of the  
115  $\Sigma N_r$  components will be compared to values reported in literature. Similar to Part I, the influence of micrometeorology on modeled fluxes and deposition velocities will be investigated. Dry depositions estimated with the EC method will be compared to results from modeling approaches using in-situ and modeled input parameters and to nitrogen throughfall measurements. We will discuss the ecological impact of nitrogen deposition on forest ecosystems. A comparison to annual N budgets reported for other forest ecosystems will be carried out.~~

## 120 2 Materials and Methods

### 2.1 Site and meteorological conditions

Measurements were made in the Bavarian Forest National Park (NPBW) (48°56'N 13°25'E, 807 m a.s.l) in southeast Germany. The unmanaged site is located in the Forellenbach catchment ( $\sim 0.69 \text{ km}^2$  (Beudert and Breit, 2010)), is surrounded by a natural, mixed forest, and is about 3 km away from the Czech border. Due to the absence of emission sources of  $\text{N}_r$  in the surroundings of the measurement site, mean annual concentrations of  $\text{NO}_2$  (2.1-4.8 ppb ( $1.2\text{-}2.8 \mu\text{g N m}^{-3}$ )),  $\text{NO}$  (0.4-1.6 ppb ( $0.2\text{-}0.9 \mu\text{g N m}^{-3}$ )) and  $\text{NH}_3$  (1.4 ppb ( $0.8 \mu\text{g N m}^{-3}$ )) are low (Beudert and Breit, 2010). The site is characterized by low annual temperatures ( $6.1^\circ\text{C}$ ) and high annual precipitation (1327 mm) measured at 945 m a.s.l. Annual temperature in 2016, 2017, and 2018 was  $6.8^\circ\text{C}$ ,  $6.9^\circ\text{C}$ , and  $8.0^\circ\text{C}$  and precipitation was 1208 mm, 1345 mm, and 1114 mm, respectively. There are no industries or power plants nearby, only small villages with moderate animal housing and farming (Beudert et al., 2018). Due to these site characteristics, measurements of the  $\Sigma\text{N}_r$  background deposition are possible. For monitoring air quality and micrometeorology a 50 m tower was installed in the 1980s. Measurements of ozone, sulphur dioxide, and  $\text{NO}_x$ , the sum of  $\text{NO}$  and  $\text{NO}_2$ , have been conducted since 1990 (Beudert and Breit, 2010). The Forellenbach site is part of the International Cooperative Program on Integrated Monitoring of Air pollution Effects on Ecosystems (ICP IM) within the framework of the Geneva Convention on Long-Range Transboundary Air Pollution (UNECE, 2021) and belongs to the Long Term Ecological Research (LTER) network (LTER, 2021). The Federal Environment Agency (UBA) and NPBW Administration have been carrying out this monitoring program in the Forellenbach catchment. The flux footprint consists of Norway spruce (*Picea abies*) and European beech (*Fagus sylvatica*) covering approximately 80% and 20% of the footprint, respectively (Zöll et al., 2019). During the study period, maximum stand height was less than 20 m since the dominating Norway spruce is recovering from a complete dieback by bark beetle in the mid-1990s and 2000s (Beudert and Breit, 2014).

### 140 2.2 Experimental setup

Flux measurements of  $\Sigma\text{N}_r$  were made from January 2016 until end of June 2018 at a height of 30 m above ground. A custom-built  $\Sigma\text{N}_r$  converter (total reactive atmospheric nitrogen converter, TRANC) after Marx et al. (2012) and a 3-D ultrasonic anemometer (GILL-R3, Gill Instruments, Lymington, UK) were attached on different booms close to each other at 30 m height. The horizontal and vertical sensor separations were 32 cm and 20 cm, respectively (Wintjen et al., 2020). The TRANC was connected via a 45 m opaque PTFE tube to a fast-response chemiluminescence detector (CLD 780 TR, ECO PHYSICS AG, Dürnten, Switzerland), which was housed in an air-conditioned box at the bottom of the tower. The CLD was coupled to a dry vacuum scroll pump (BOC Edwards XDS10, Sussex, UK), which was placed at ground level, too. The inlet of the TRANC is designed after Marx et al. (2012) and Ammann et al. (2012). The conversion of  $\Sigma\text{N}_r$  to  $\text{NO}$  is split in two steps. First, a thermal conversion occurs in an iron-nickel-chrome tube at  $870^\circ\text{C}$  leading to a split up of  $\text{NH}_4^+$  and  $\text{NO}_3^-$  aerosols such as ammonium sulfate, ammonium nitrate, sodium and calcium nitrate into their subcomponents. In case of  $\text{NH}_4\text{NO}_3$ , it is thermally converted to  $\text{NH}_3$  and  $\text{HNO}_3$  (Marx et al., 2012). The latter is split up into  $\text{NO}_2$ ,  $\text{H}_2\text{O}$ , and  $\text{O}_2$ .  $\text{NH}_3$  is oxidized by  $\text{O}_2$  at a platinum gauze to  $\text{NO}$ .  $\text{HONO}$  is split up to  $\text{NO}$  and a hydroxyl radical ( $\text{OH}$ ). In a second step, a gold tube passively

heated to 300°C catalytically converts the remaining oxidized  $N_r$  species to NO. In this process, carbon monoxide (CO) is acting as a reducing agent. More details about the chemical conversion steps can be found in Marx et al. (2012). A critical orifice was mounted at the TRANC's outlet and restricted the mass flow to  $2.1 \text{ L min}^{-1}$  after the critical orifice assuring low pressure along the tube. The pressure gradient from the critical orifice to the CLD was not measured. Thus, only assumptions about the turbulent flow regime can be made. Considering tube length and lag time minus residence time in the converter, the latter assumed to 2 sec at maximum due to tube length and platinum mesh as an additional flow resistance, flow speed was at  $2.7 \text{ ms}^{-1}$  at maximum. Using an inner diameter of 4.4 mm and a kinematic viscosity at 15°C ( $1.485 \cdot 10^{-5} \text{ m}^2 \text{ s}^{-1}$ ), we calculated a Reynolds number of 800 indicating an overall laminar flow. We cannot provide a reasonable explanation to the low Reynolds number since pressure gradient was not measured. Generally, the flow type inside the tube affects high-frequency attenuation (Massman, 1991; Lenshow and Raupach, 1991; Moncrieff et al., 1997). High-frequency attenuation was corrected with an empirical method based fully on measured cospectra (Wintjen et al., 2020). Since an empirical approach was used to estimate the high-frequency damping, effects originating from the low Reynolds number and from physical and chemical processes occurred after the critical orifice were considered in the flux analysis.

The conversion efficiency of the TRANC had been investigated by Marx et al. (2012). They found 99% for  $\text{NO}_2$ , 95% for  $\text{NH}_3$ , and 97% for a gas mixture of  $\text{NO}_2$  and  $\text{NH}_3$ . Conversion efficiencies for sodium nitrate ( $\text{NaNO}_3$ ), ammonium nitrate ( $\text{NH}_4\text{NO}_3$ ), and ammonium sulfate ( $(\text{NH}_4)_2\text{SO}_4$ ) were 78%, 142%, and 91%, respectively. Overall, the results indicate that the TRANC is able to convert aerosols and gases efficiently to NO. For further details we refer to the publication of Marx et al. (2012).

For determining local turbulence - wind speed, wind direction, friction velocity ( $u_*$ ) - measurements of the wind components ( $u$ ,  $v$ , and  $w$ ) were conducted using the sonic anemometer. Close to the sonic, an open-path LI-7500 infrared gas analyzer (IRGA) for measuring  $\text{CO}_2$  and  $\text{H}_2\text{O}$  concentrations was installed.

For investigating the local meteorology, air temperature and relative humidity sensors (HC2S3, Campbell Scientific, Logan, Utah, USA) were mounted at four different heights (10, 20, 40, and 50 m above ground). At the same levels, wind propeller anemometers (R.M. Young, Wind Monitor Model 05103VM-45, Traverse City, Michigan, USA) were mounted on booms. Leaf wetness sensors designed after the shape of a leaf (Decagon, LWS,  $n=6$ , Pullman, Washington, USA) were attached to branches of a spruce and a beech tree near the tower. Sensors of the beech tree were at heights of approximately 2.1 m, 5.6 m, and 6.1 m, sensors of the spruce tree were at heights of 2.1 m, 4.6 m, and 6.9 m. These measurements started in April 2016. Due to a wetting of the sensor's surface, the electric conductivity of the material changes. This signal, the leaf wetness, was converted by the instrument to dimensionless counts. Based on the number and range of counts, different wetness states could be defined. Half-hourly leaf wetness values were in the range from 0 to 270. In this study, we defined the wetness states "dry" and "wet". The condition wet can be induced by the accumulation of hygroscopic particles extending the duration of the wetness state or water droplets. In order to classify a leaf as dry or wet, we determined a threshold value based on the medians of leaf wetness values. During daylight (global radiation  $> 20 \text{ W m}^{-2}$ ), medians ranged from 1.1 to 2.0 and were between 4.1 and 9.4 during nighttime. During nighttime, medians are higher due to dew formation. According to the values determined during daylight, we set the threshold value to 1.5 for all sensors. If the leaf wetness value was lower than 1.5, the leaf was considered as

dry. Otherwise, the leaf surface was considered as wet. To take differences between the sensors into account, all sensors were used to derive a common wetness Boolean. Therefore, the number of dry sensors were counted for each half-hour: If at least three sensors were considered as dry, the corresponding half-hour was considered as mostly dry. A cleaning of sensors was not conducted because contamination effects could be corrected by implemented algorithms. The derived wetness Boolean was used in the analysis of deposition velocities (Sec. 3.3).

Ambient  $\text{NH}_3$  was collected by passive samplers at ground level (1.5), 10, 20, 30, and 50 m from January 2016 to June 2018. Measurements at 40 m started in July 2016. The collector at ground level was moved to 40 m. Passive samplers of the IVL type (Ferm, 1991) were used for  $\text{NH}_3$ , and the exposure duration was approximately one month at a time. DELTA measurements (DENuder for Long-Term Atmospheric sampling (e.g., Sutton et al., 2001; Tang et al., 2009)) of  $\text{NH}_3$ ,  $\text{HNO}_3$ ,  $\text{SO}_2$ ,  $\text{NO}_3^-$ , and  $\text{NH}_4^+$  were taken at the 30-m platform. The DELTA measurements had the same sampling duration as the passive samplers. The denuder preparation and subsequent analyzing of the samples was identical to the procedure for KAPS denuders (Kananaskis Atmospheric Pollutant Sampler, (Peake, 1985; Peake and Legge, 1987)) given in Dämmgen et al. (2010) and Hurkuck et al. (2014). Basic denuders were coated with sodium carbonate to collect  $\text{HNO}_3$ ,  $\text{SO}_2$ , and  $\text{HCl}$ . Citric acid was applied to acid denuders for removing  $\text{NH}_3$ . Two cellulose filter papers (Whatman No. 1, 25 mm diameter) were used for collecting aerosols. The first filter was prepared with potassium carbonate in glycerol, the second filter with citric acid. During operation, we controlled the pump to keep flow at a constant level and checked the pipes for contamination effects before analyzing. Blank values were used as additional quality control.

Additionally, fast-response measurements of  $\text{NH}_3$  were performed with a  $\text{NH}_3$  Quantum Cascade Laser (QCL) (model mini QC-TILDAS-76 from Aerodyne Research, Inc. (ARI, Billerica, MA, USA)) at 30 m height, ~~too~~. The setup of the QCL was the same as described in Zöll et al. (2016). In contrast to Zöll et al. (2016), we were not able to calculate  $\text{NH}_3$  fluxes with the QCL using the EC method (see Sec. 2.3). Further details about the location and specifications of the installed instruments can be found in Zöll et al. (2019) and Wintjen et al. (2020).

At the top of the tower (50-m platform), measurements of  $\text{NO}_2$  and  $\text{NO}$  were conducted by the NPBW using a chemiluminescence detector (APNA - 360, HORIBA, Tokyo, Japan). The instrument was equipped with a thermal  $\text{NO}_x$  converter resulting in cross-sensitivity to higher oxidized nitrogen compounds. Measurements of global radiation and atmospheric pressure were also conducted at 50 m. Above the canopy, the concentration gradients of  $\text{NO}_2$  and  $\text{NO}$  were probably not significant. Seok et al. (2013) found highest  $\text{NO}_x$  concentrations above the canopy but concentration gradients were negligible at this height. Since both measurement heights were above the canopy, no correction was applied to  $\text{NO}_2$  and  $\text{NO}$  concentration measurements. Precipitation was measured at a location in 1 km southwest distance from the tower according to WMO (World Meteorological Organization) guidelines (Jarraud, 2008). Wet deposition was collected as bulk and wet-only samples in weekly intervals in close vicinity to the tower using four samplers, three bulk samplers and one wet-only sampler, at an open site. A detailed description of the wet deposition measurements is given as supplemental material A1.

## 220 2.3 Flux calculation and post processing

The software package EddyMeas, included in EddySoft (Kolle and Rebmann, 2007), was used to record the data with a time resolution of 10 Hz. Analog signals from CLD, LI-7500, and the sonic anemometer were collected at the interface of the anemometer and joined to a common data stream. Flux determination covered the period from 1 January 2016 to 30 June 2018. Half-hourly fluxes were calculated by the software EddyPro 7.0.4 (LI-COR Biosciences, 2019). For flux calculation a 2-D  
225 coordinate rotation of the wind vector was selected (Wilczak et al., 2001), spikes were detected and removed from time series after Vickers and Mahrt (1997), and block averaging was applied. Due to the distance from the TRANC inlet to the CLD, a time lag between concentration and sonic data was inevitable. The covariance maximization method allows to estimate the time lag via shifting the time series of vertical wind and concentration against each other until the covariance is maximized (Aubinet et al., 2012; Burba, 2013). The time lag was found to be approximately 20 s (see Fig. S1 of the Supplementary Material). We  
230 instructed EddyPro to compute the time lag after covariance maximization with default setting while using 20 s as default value and set the range from 15 s to 25 s (for details see Wintjen et al., 2020). For correcting flux losses in the high-frequency range we used an empirical method suggested by Wintjen et al. (2020), which uses measured cospectra of sensible heat ( $Co(w, T)$ ) and  $\Sigma N_r$  flux ( $Co(w, \Sigma N_r)$ ) and an empirical transfer function. We followed their findings and used medians of the damping factors calculated for correcting calculated fluxes since the chemical composition of  $\Sigma N_r$  exhibits seasonal differences (see  
235 Fig. 3 and Brümmer et al., 2013). Each damping factor (median) refers to period of two month. On average, the damping factor was 0.78, which corresponds to flux loss of 22% (Wintjen et al., 2020). The authors determined flux loss factors for two different ecosystems, which are different, for example, in the composition of  $\Sigma N_r$ . They assumed that the differences in flux losses are also related to the chemical composition of  $\Sigma N_r$ . The low-frequency flux loss correction was done with the method of Moncrieff et al. (2004), and the random flux error was calculated after Finkelstein and Sims (2001).

240 Previous measurements with the same CLD model by Ammann et al. (2012) and Brümmer et al. (2013) revealed that the device is affected by ambient water vapour due to quantum mechanical quenching. Excited  $NO_2$  molecules can reach ground state without emitting a photon by colliding with a  $H_2O$  molecule, thereby no photon is detected by the photo cell. It results in a sensitivity reduction of 0.19% per  $1 \text{ mmol mol}^{-1}$  water vapour increase. Thus, calculated fluxes were corrected after the approach by Ammann et al. (2012) and Brümmer et al. (2013) using the following equation:

$$245 F_{NO, \text{int}} = -0.0019 \cdot c_{\Sigma N_r} \cdot F_{H_2O} \quad (1)$$

The  $NO$  interference flux  $F_{NO, \text{int}}$  has to be added to every estimated flux value.  $c_{\Sigma N_r}$  is the measured concentration of the CLD and  $F_{H_2O}$  the estimated  $H_2O$  flux from the LI-7500 eddy-covariance system. The correction contributed approximately  $132 \text{ g N ha}^{-1}$  to two years of TRANC flux measurements if the Mean-Diurnal-Variation (MDV) approach was used as gap-filling approach. Half-hourly interference fluxes were between  $-3$  and  $+0.3 \text{ ng N m}^{-2} \text{ s}^{-1}$ . Their random flux uncertainty ranged  
250 between  $0.0$  and  $0.5 \text{ ng N m}^{-2} \text{ s}^{-1}$ . Since we measured  $H_2O$  fluxes with an open-path system and used them for correcting  $\Sigma N_r$  fluxes, density corrections following the Webb-Pearman-Leuning correction for  $H_2O$  fluxes measured with closed-path systems (Ibrom et al., 2007) were not accounted for. The impact on the correction is likely small, but the determined interference flux correction should be seen as an upper estimate.



After flux calculation, we applied different criteria to identify low-quality fluxes. We removed fluxes, which were outside  
255 the predefined flux range of  $-520 \text{ ng N m}^{-2} \text{ s}^{-1}$  to  $420 \text{ ng N m}^{-2} \text{ s}^{-1}$  (I), discarded periods with insufficient turbulence  
( $u_* < 0.1 \text{ m s}^{-1}$ ) (see Zöll et al., 2019) (II), and fluxes with a quality flag of "2" (Mauder and Foken, 2006) (III). In order  
to avoid uncertainties due to the washout process as it introduces an additional sink below the measurement height leading  
to a height dependent flux, we applied a precipitation filter on  $\Sigma N_r$  flux measurements (IV). These criteria ensure the quality  
of the fluxes, but lead to systematic data gaps in flux time series. Flux data with applied  $u_*$ -filter were used for investigating  
260 the flux pattern of  $\Sigma N_r$ . Figures 4, 5, 7, S5, S6, S9, S10, S12, S13, and associated descriptions are based on this flux data  
set. Instrumental performance problems led to further gaps in the time series. Most of them were related to maintaining  
and repairing of the TRANC and/or CLD, for example, heating and pump issues, broken tubes, empty  $\text{O}_2$  gas tanks ( $\text{O}_2$  is  
required for CLD operation), power failure, or a reduced sensitivity of the CLD. The reduction in sensitivity may be caused  
by reduced pump performance leading to an increase in sample cell pressure. If pressure in the sampling cell is outside the  
265 regular operating range, low pressure conditions needed for the detection of photons emitted by excited  $\text{NO}_2$  molecules may  
not hold. We checked the pressure in the sample cell of the CLD during each, at least monthly, site visit. If the sample cell  
pressure was outside the allowed range, tip seals of the pump were replaced. The sensitivity of the CLD could also be reduced  
by changes in the  $\text{O}_2$  supply from gas tanks to ambient, dried box air if  $\text{O}_2$  gas tanks were empty. Issues in the air-conditioning  
system of the box could also affect the sensitivity of the CLD. An influence of aging on the inlet, tubes, and filters may also  
270 affect the measurements. In order to minimize an impact on the measurements, half-hourly raw concentrations were carefully  
checked for irregularities like spikes or drop-outs by visual screening. Considering the time period of ongoing measurements  
from the beginning of January 2016 till June 2018, the quality flagging resulted in 58.6% missing data. The loss in flux data is  
higher than values reported by Brümmer et al. (2013). They reported a flux loss of 24% caused by  $u_*$  filtering. In this study,  
the same  $u_*$  threshold caused a flux loss of approximately 15.5%. 32.7% data loss from January 2016 to June 2018 was caused  
275 by instrumental performance problems showing that TRANC-CLD system was overall operating moderately stable. For gap-  
filling we applied the MDV approach to gaps in the  $\Sigma N_r$  flux time series. The window for filling each gap was set to  $\pm 5$  days.  
Remaining, long-term gaps were filled by a monthly average of the specific half-hour value estimated from non-gap-filled  
fluxes (Fig. 5) in order to estimate  $\Sigma N_r$  dry deposition sums from June 2016 to May 2017 and from June 2017 to May 2018.  
Uncertainties of the gap-filled fluxes are estimated by the standard error of the mean.

280 Hereafter, we named this MDV approach "original" (OMDV). To examine the impact of the  $u_*$ -filter as it may remove  
preferentially smaller fluxes occurring at low turbulent conditions, we compared dry deposition sums calculated with and  
without  $u_*$ -filter while using OMDV. On both datasets, flux filters (I), (III), and (IV) were applied (see Fig. 8 and associated  
text). Seasonal and annual  $\Sigma N_r$  dry depositions shown in Table 1 referred to flux data with  $u_*$ -filter and were calculated by  
using OMDV.

285 In addition to  $u_*$ , other micrometeorological parameters may also bias annual dry deposition. Therefore, we examined the  
impact of temperature, relative humidity, and wind speed on the dry deposition sums of  $\Sigma N_r$  compared to the dry deposition  
when using OMDV as gap-filling approach. We named this gap-filling approach as "conditional" MDV (CMDV) and applied  
it to flux data with and without  $u_*$ -filter. For CMDV, we considered only fluxes in the time frame of  $\pm 5$  days, at which

temperature agreed within  $\pm 3^\circ\text{C}$ , relative humidity by  $\pm 5\%$ , or wind speed by  $\pm 1.5 \text{ m s}^{-1}$ . Remaining, long-term gaps were  
290 treated similar to OMDV.

As outlined in Sec. 2.2, measurements of  $\text{NH}_3$  were made with a QCL at high temporal resolution. In combination with the  
sonic anemometer, it gives the opportunity to determine  $\text{NH}_3$  fluxes and to further investigate the non- $\text{NH}_3$  component of  
the  $\Sigma\text{N}_r$  flux. However, a calculation of the  $\text{NH}_3$  fluxes with the EC method was not possible in this study. No consistent  
 $\text{NH}_3$  time lag was found making flux evaluation impossible. Due to regular pump maintenance, cleaning of the inlet and  
295 absorption cell, issues related to the setup of the QCL were unlikely to be the cause. We suppose that the variability in the  
measured  $\text{NH}_3$  concentrations was not sufficiently detectable by the instrument. Significant short-term variability in the  $\Sigma\text{N}_r$   
raw concentrations were not found in the  $\text{NH}_3$  signal even in spring or summer. Thus, no robust time lag estimation could be  
applied to the vertical wind component of the sonic anemometer and the  $\text{NH}_3$  concentration. Recently, Ferrara et al. (2021)  
found large uncertainties for low  $\text{NH}_3$  fluxes measured with the same QCL model. Cross-covariance functions had a low  
300 signal-to noise ratio indicating that most of the fluxes were close to the detection limit.

#### 2.4 Determining deposition velocity of $\Sigma\text{N}_r$ from measurements

In surface-atmosphere exchange models of  $\text{N}_r$  species like  $\text{NO}_2$ ,  $\text{NO}$ ,  $\text{NH}_3$ ,  $\text{HNO}_3$ , or **nitrogen-aerosols related aerosol com-  
pounds**, the flux ( $F_t$ ) is calculated by multiplying concentrations of a trace gas modeled or measured at a reference height  
( $\chi_a(z-d)$ ) with a so-called deposition velocity ( $v_d(z-d)$ ) where  $z$  is measurement height and  $d$  the zero-plane displacement  
305 height (van Zanten et al., 2010). The deposition velocity can be described by an electrical analogy and is defined as the inverse  
of the sum of three resistances (Wesely, 1989; Erisman and Wyers, 1993). According to its definition a positive  $v_d$  indicates  
deposition, a negative  $v_d$  emission. Note that, strictly speaking, for bidirectional exchange  $v_d$  needs to be interpreted as an  
“exchange velocity”, i.e. it can technically become negative during emission phases. Equations are the same as for  $v_d$  (van  
Zanten et al., 2010).

$$310 \quad F_t = -v_d(z-d) \cdot \chi_a(z-d) \quad \text{with } v_d = (R_a(z-d) + R_b + R_c)^{-1} \quad (2)$$

$R_a$  is the aerodynamic resistance,  $R_b$  is the quasi-laminar boundary layer resistance, and  $R_c$  is the canopy resistance.  $R_a$   
is influenced by turbulent characteristics (Paulson, 1970; Webb, 1970; Garland, 1977) and  $R_b$  (Jensen and Hummelshøj,  
1995, 1997) depends on surface characteristics and chemical properties of the gas or particle of interest. Both have in com-  
mon that they are proportional to the inverse of  $u_*$ .  $R_c$  consists of several parallel connected resistances describing the ex-  
315 change with the vegetated surface (van Zanten et al., 2010). **Further details about the implementation of these resistances in  
surface-atmosphere models can be found in van Zanten et al. (2010).**

### 3 Results

#### 3.1 Measured concentrations, deposition velocities, and fluxes of $\Sigma N_r$ and individual $N_r$ compounds during the measurement campaign

320 Figure 1 shows ambient concentrations of  $\Sigma N_r$  (black),  $NH_3$  (red) and  $NO_x$  (blue) as half-hourly averages for the entire measurement campaign. Data gaps were related to instrumental performance problems. No  $\Sigma N_r$  measurements were possible until end of May 2016 due to heating problems of the TRANC. A breakdown of  $\Sigma N_r$  in compounds contributing most to its concentration pattern is shown in Fig. 2, which illustrates a comparison of  $\Sigma N_r$  concentrations with DELTA denuder and  $NO_x$  measurements on monthly basis.

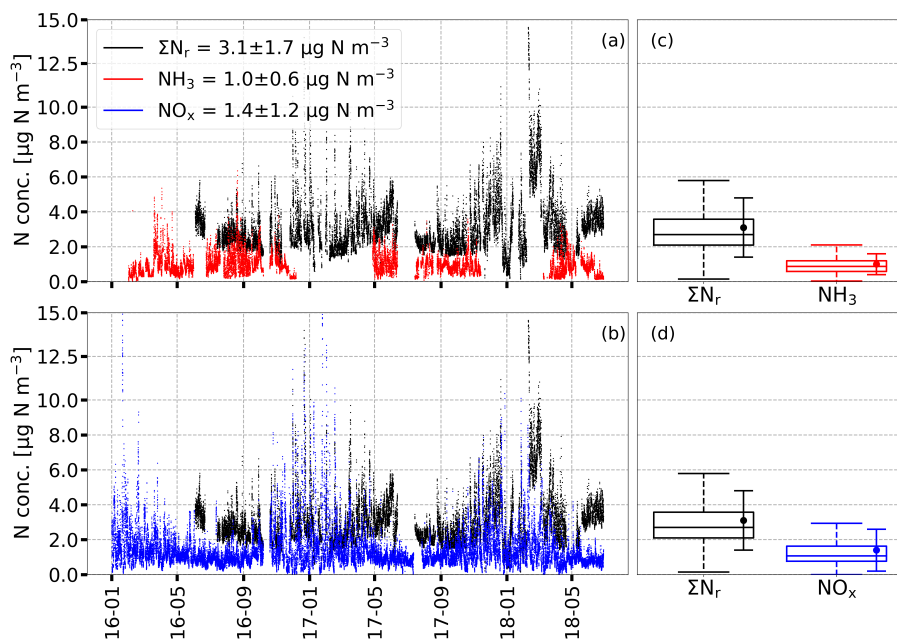


**Figure 1.** Half-hourly averaged concentrations of  $\Sigma N_r$  (black),  $NH_3$  (red) and  $NO_x$  (blue) in  $\mu g N m^{-3}$  from 1 January 2016 to 30 June 2018 displayed in (a) and (b). Box plots (box frame = 25 % to 75 % interquartile range (IQR), bold line = median, whisker =  $1.5 \cdot IQR$ ) with average values (dots) shown in (c) and (d) refer to the entire campaign. Error bars represent one standard deviation. Y-axis is capped at  $15 \mu g N m^{-3}$ .

325  $\Sigma N_r$  concentrations exhibited highest values during the winter months. For example, values were higher than  $10 \mu g N m^{-3}$  during January 2017 and February 2018.  $NO_x$  also showed a relatively high concentration level during winter, too. During spring and summer,  $NO_x$  values were lower than  $2 \mu g N m^{-3}$  and hence, their contribution to  $\Sigma N_r$  decreased. However,  $\Sigma N_r$  values remained around  $3 \mu g N m^{-3}$  and reached values of up to  $6 \mu g N m^{-3}$ , which was related to higher  $NH_3$  concentrations during these periods. The  $\Sigma N_r$  concentration was  $3.1 \mu g N m^{-3}$  on average,  $NH_3$  was  $1.0 \mu g N m^{-3}$ , and  $NO_x$  was  $1.4 \mu g N$   
330  $m^{-3}$  on average with the latter values being in agreement with concentrations reported by Beudert and Breit (2010). Averaged

NH<sub>3</sub> concentrations of the QCL agreed well with NH<sub>3</sub> from passive samplers and DELTA measurements (Fig. S2). Overall, the agreement in the annual pattern was ~~good~~ reasonable, but a bias between the QCL and the diffusion samplers was found. From passive sampler measurements, an increase in the NH<sub>3</sub> concentration with measurement height ~~could be~~ was observed. At 10 m (in the canopy), the lowest NH<sub>3</sub> concentrations were measured. No systematic difference was found between 20 m and 30 m. At 50 m, the NH<sub>3</sub> concentration ~~was higher~~ exceeded that at 30 m by 0.1 µg N m<sup>-3</sup> ~~than at 30 m~~. During winter, the difference in measurement heights diminished.

The ~~observations made for the~~ seasonal ~~changes~~ variations of the half-hourly ΣN<sub>r</sub> concentrations are ~~also visible for their monthly medians (Fig. S3). Figure S3 shows monthly box plots of the concentrations~~ represented by box-and-whisker plots including monthly medians in Fig. S3. In general, median concentrations were comparable for the entire campaign with slight differences between the years. Medians ~~were~~ ranged between 2 and 3.5 µg N m<sup>-3</sup>. From July to September, concentrations were slightly higher in 2016 than in 2017. During this period, IQRs and whiskers were the smallest for the entire year showing less variability in ΣN<sub>r</sub> concentrations. In spring and winter, median concentrations were higher, and concentrations covered a wider range compared to the summer month. Figure S4 shows the corresponding diurnal patterns for each month. During the entire day, ΣN<sub>r</sub> concentrations exhibited variations of less than 1 µg N m<sup>-3</sup>. If concentrations were averaged for each season (not shown), higher concentrations were observed from 9:00 to 15:00 LT and lower values during the night.

Figure 2 shows absolute concentrations of individually measured N<sub>r</sub> compounds as stacked bars and ΣN<sub>r</sub> from the TRANC from January 2016 to June 2018. TRANC and NO<sub>x</sub> measurements were averaged to exposure periods of DELTA measurements. DELTA measurements recorded at an insufficient pump flow were excluded from the analysis. Missing NH<sub>3</sub> values in the DELTA time series were filled by NH<sub>3</sub> data determined from the passive sampler mounted at 30 m. Remaining data gaps in the DELTA time series of NH<sub>3</sub>, HNO<sub>3</sub>, NH<sub>4</sub><sup>+</sup>, and NO<sub>3</sub><sup>-</sup> were replaced by monthly averages from other years.

The comparison of the TRANC with DELTA+NO<sub>x</sub> revealed overestimations by the latter from August 2016 to October 2016 and from January to March 2017. On average, an underestimation by DELTA+NO<sub>x</sub> of approximately 0.41 µg N m<sup>-3</sup> with a standard deviation of 0.93 µg N m<sup>-3</sup> was observed. The median value was about 0.4 µg N m<sup>-3</sup>.

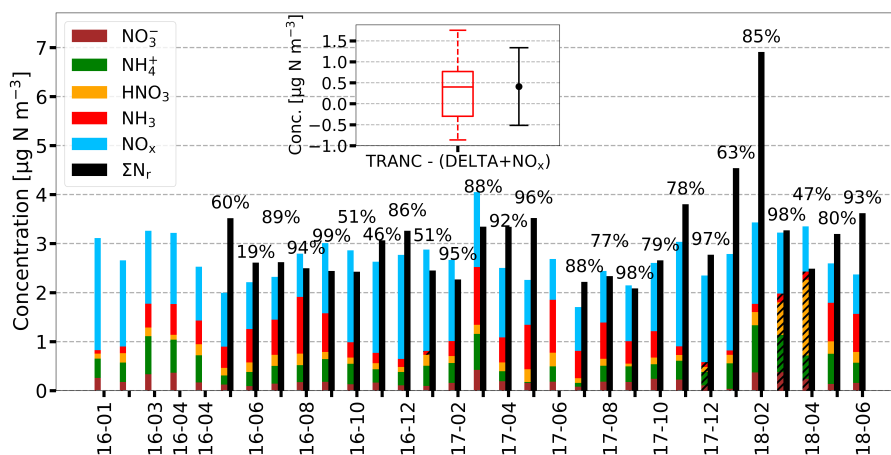


**Figure 2.** Monthly stacked concentration of TRANC, DELTA, and  $\text{NO}_x$  in  $\mu\text{g N m}^{-3}$  for the entire measurement campaign. Missing  $\text{NH}_3$  measurements values from the DELTA measurements caused by a low pump flow were filled with passive sampler values from 30 m. This procedure was done for December 2016 and 2017, March 2018, and April 2018. Remaining gaps in the time series of  $\text{HNO}_3$ ,  $\text{NH}_4^+$ , and  $\text{NO}_3^-$  were replaced by monthly averages estimated from other years if possible. In case of  $\text{NH}_3$ , the procedure was applied to January 2017. For the other compounds, the gap-filling was done for December 2017, March 2018, and April 2018. Gap-filled bars are hatched.  $\text{NO}_x$  and  $\Sigma\text{N}_r$  were averaged to the exposure periods of the DELTA samplers. Numbers above the bars indicate the relative coverage of TRANC measurements during each exposure period.

$\text{HNO}_3$ ,  $\text{NH}_4^+$ , and  $\text{NO}_3^-$  concentrations were nearly equal through the entire measurement campaign. Seasonal differences existed mainly for  $\text{NH}_3$  and  $\text{NO}_x$ . We measured average concentrations of 0.55, 0.17, 0.42, 0.19, and  $1.40 \mu\text{g N m}^{-3}$  for  $\text{NH}_3$ ,  $\text{HNO}_3$ ,  $\text{NH}_4^+$ ,  $\text{NO}_3^-$ , and  $\text{NO}_x$  for the entire campaign, respectively. On average, the relative contribution of  $\text{NH}_3$ ,  $\text{HNO}_3$ ,  $\text{NH}_4^+$ , and  $\text{NO}_3^-$  to  $\Sigma\text{N}_r$  was less than 50% for the entire measurement campaign as visualized by Fig. 3. We further observed a low particle contribution to the  $\Sigma\text{N}_r$  concentrations ( $\sim 22\%$  on average) showing that the  $\Sigma\text{N}_r$  concentration pattern was significantly influenced by gaseous  $\text{N}_r$  compounds.

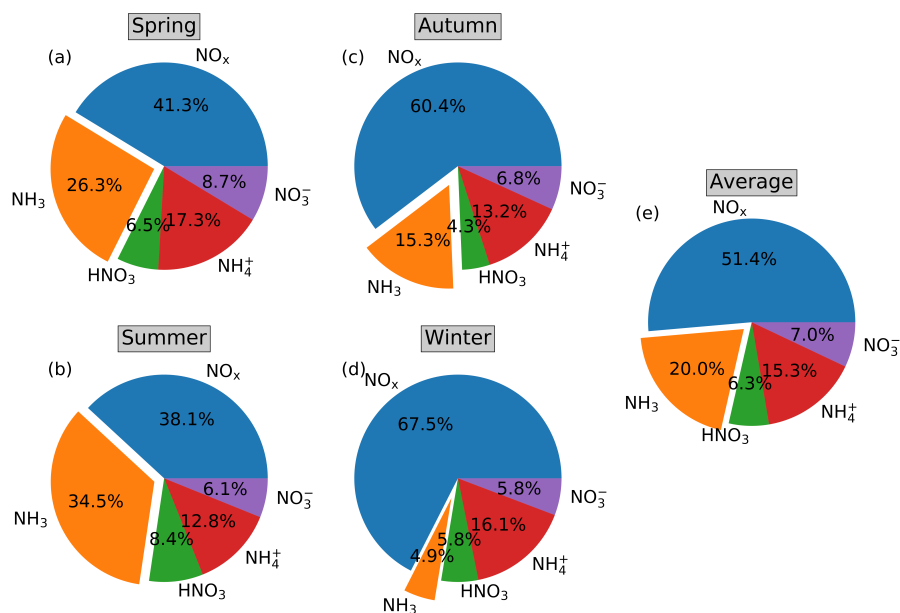


**Figure 3.** Pie charts showing the relative contribution of concentrations for NO<sub>x</sub>, NH<sub>3</sub>, NO<sub>3</sub><sup>-</sup>, NH<sub>4</sub><sup>+</sup>, and HNO<sub>3</sub> to  $\Sigma N_r$  based on DELTA samplers and NO<sub>x</sub> measurements for different seasons of the year. NO<sub>x</sub> measurements are averaged to exposure periods of the DELTA samplers. (a) to (d) refer to spring, summer, autumn, and winter, respectively. (e) shows the average relative contribution to  $\Sigma N_r$  for the entire measurement period.

360 In general, NO<sub>x</sub> showed the highest contribution to  $\Sigma N_r$  and followed seasonal changes with highest values during winter and lowest values in summer. NH<sub>3</sub> showed also featured seasonal changes variations with concentrations lowest in winter and highest values in spring and summer. Seasonal contributions of HNO<sub>3</sub> varied by less than 2% compared to the average. The highest relative contribution of HNO<sub>3</sub> was found for summer. NO<sub>3</sub><sup>-</sup> and NH<sub>4</sub><sup>+</sup> exhibited highest values for spring. The excess of NH<sub>4</sub><sup>+</sup> over NO<sub>3</sub><sup>-</sup> is obvious. Similar to HNO<sub>3</sub>, the seasonal contribution of NO<sub>3</sub><sup>-</sup> and NH<sub>4</sub><sup>+</sup> deviated only by  $\pm 2\%$  from their averages. Only small seasonal changes in the overall  $\Sigma N_r$  concentration were observed. As seen by shown in Fig. 2,  $\Sigma N_r$  concentrations were between 2 and 4.5  $\mu\text{g N m}^{-3}$  excluding February 2018. We measured 3.3, 2.6, 2.5, and 3.0  $\mu\text{g N m}^{-3}$  with the TRANC system for spring, summer, autumn, and winter, respectively.

### 3.2 Measured exchange fluxes and deposition velocities of $\Sigma N_r$

Figure 4 shows the non-gap-filled  $\Sigma N_r$  fluxes depicted as box plots on a monthly time scale. The convention is as follows:  
 370 negative fluxes represent deposition, positive fluxes emission.

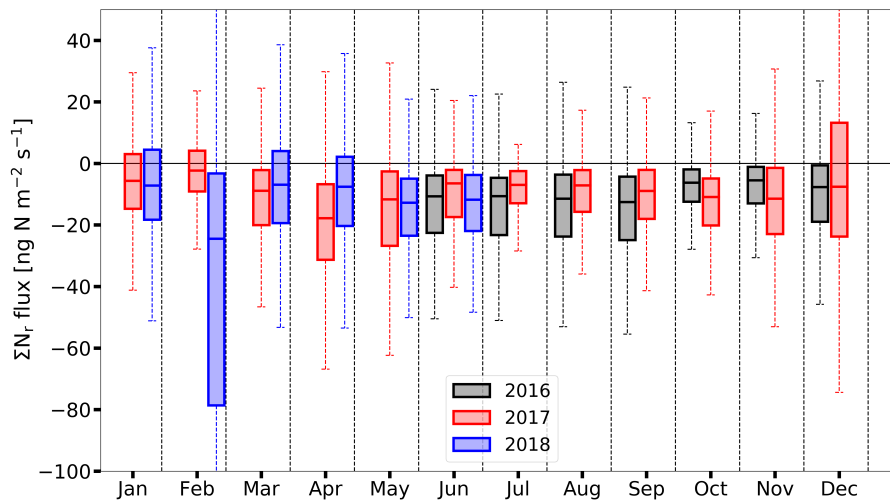


**Figure 4.** Time series of measured high-quality (flags "0" and "1")  $\Sigma N_r$  fluxes depicted as box-and-whisker plots on monthly basis (box frame = 25% to 75% interquartile ranges (IQR), bold line = median, whisker = 1.5 · IQR) in  $\text{ng N m}^{-2} \text{s}^{-1}$ . Colors indicate different years. The whiskers in February 2018 cover the range from -191 to 105  $\text{ng N m}^{-2} \text{s}^{-1}$ , the upper whisker of December 2017 was at 69  $\text{ng N m}^{-2} \text{s}^{-1}$ .

Except for February 2018, all  $\Sigma N_r$  flux medians were between -15 and -5  $\text{ng N m}^{-2} \text{s}^{-1}$  indicating that deposition of  $\Sigma N_r$  predominated at our measurement site. Quality assured half-hourly fluxes showed 80% deposition and 20% emission fluxes. On a half-hourly basis, fluxes were in the range from -516 to 399  $\text{ng N m}^{-2} \text{s}^{-1}$ . On a monthly basis, random flux error medians were between 3 and 6  $\text{ng N m}^{-2} \text{s}^{-1}$ . According to Langford et al. (2015), the limit of detection (LOD) is calculated by multiplying ~~1.96 with~~ the random flux error (95% confidence limit) with 1.96. The comparison of half-hourly fluxes with their individual LOD revealed that 79% of the measured fluxes were above their detection limits. Deposition fluxes contributed with 84% to fluxes above the LOD. The fraction of emission was estimated to 16%. The relative contribution of emission fluxes to measured fluxes decreased under the consideration of the LOD. ~~It shows~~ This indicates that emission fluxes were closer to the flux detection limit of the instrument.

In general, median deposition was ~~on the same level within the same range~~ for the entire campaign with only small seasonal differences. For instance, median deposition was higher during spring and summer than during winter for 2016. However, median deposition during winter 2017 was comparable to median deposition in summer 2017. Median deposition was significantly ~~stronger increased~~ from June 2016 till September 2016 than for the same period in 2017 ~~and~~ IQR and whisker also covered a wider range, ~~too~~ in 2016. The pattern changed for the time period from October to December. In December 2017, the IQR expanded in the positive range indicating emission events for a significant time period. The largest median deposition with 25  $\text{ng N m}^{-2} \text{s}^{-1}$  and the widest range in IQR reaching approximately -80  $\text{ng N m}^{-2} \text{s}^{-1}$  were registered in February 2018 indicating strong deposition phases during that month with sporadic emission events. Such phenomena were not observed

in the years before. In the following month, the deposition was higher from March to April 2017 than for the same period in 2018. Fig. 5 shows averaged **daily diurnal** cycles of measured  $\Sigma N_r$  fluxes for every month.

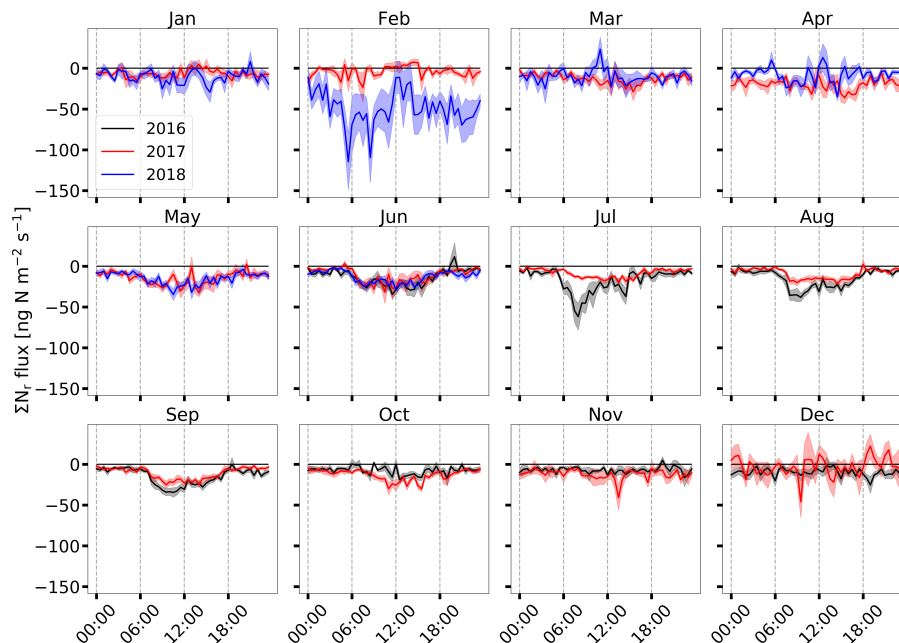


**Figure 5.** Mean **daily diurnal** cycle of  $\Sigma N_r$  fluxes ( $\text{ng N m}^{-2} \text{s}^{-1}$ ) based on half-hourly measurements for every month of  $\Sigma N_r$  fluxes from June 2016 to June 2018 **on-half-hourly-basis**. The shaded area represents the standard error of the mean. Colors indicate different years.

390 In general, the  $\Sigma N_r$  **daily diurnal** cycle exhibited low deposition or **neutral-exchange** fluxes close to zero during night-time/evening and increasing deposition during daytime. Deposition **rates** fluxes were similar during the night for the entire campaign except for February 2018. Maximum deposition was reached between 9:00 and 15:00 LT. Deposition is enhanced from May until September showing fluxes between -40 and -20  $\text{ng N m}^{-2} \text{s}^{-1}$ . From October to November and from December to February, the **daily diurnal** cycle weakened with **neutral** near-zero or small negative fluxes, which were lower than -10  $\text{ng N}$   
 395  $\text{m}^{-2} \text{s}^{-1}$ . The **daily diurnal** cycles of the respective same months were **uniform comparable**. However, during certain months, which differ in their micrometeorology and/or in the composition of  $\Sigma N_r$ , differences can be significant. For example, the **daily diurnal** cycles of March and April 2017 **was were** clearly different to **daily the diurnal** cycles of March and April 2018. During spring 2017, deposition fluxes were found whereas the  $\Sigma N_r$  exchange was close to **neutral-a zero one** year later. The median deposition was also larger in March and April 2017 than in the year after (Fig. 4). In December 2017, the **daily diurnal** cycle  
 400 was close to the zero line and positive fluxes were observed, although standard errors were relatively large ( $\pm 11.5 \text{ ng N m}^{-2} \text{s}^{-1}$  on average). In December 2016, small deposition fluxes were observed for the entire **daily diurnal** cycle. The **daily diurnal** cycle of February 2018 showed highest deposition values during the entire day, even the highest values during the measurement campaign. Again, **the** average standard error was relatively large ( $\pm 19.9 \text{ ng N m}^{-2} \text{s}^{-1}$ ) for February 2018 compared to February 2017.



405 Figure S5 shows the median  $v_d$  for the corresponding fluxes. Values ranged between 0.2 and 0.5  $\text{cm s}^{-1}$  for the entire campaign. In general, median  $v_d$  followed closely the seasonality of their corresponding fluxes (Fig. 4). During autumn and winter,  $v_d$  remained stable. From May to September, ~~the curve was approximately bell-shaped. a continuous increase in  $v_d$  was observed from 6:00 a.m. until noon. A decrease in  $v_d$  followed in the late afternoon (15:00 to 18:00 LT).~~ Similar to the diurnal fluxes, maximum  $v_d$  values were reached between 9:00 and 15:00 LT. During that time, values of  $v_d$  were close to 1  $\text{cm s}^{-1}$  or  
410 even higher (Fig. S6).

### 3.3 Controlling factors of measured $\Sigma N_r$ deposition velocities

From May to September, a clear diurnal pattern was found for  $v_d$  and their corresponding fluxes (Fig. 5 and Fig. S6). It was characterized by lower deposition during the night and highest values around noon (Fig. S9). During winter, deposition fluxes were close to zero and showed no diurnal variation leading to a constantly low  $v_d$  ~~during the~~ except for midday (Fig.  
415 S10). ~~During that time, a strong decrease in  $v_d$  was found with near-zero or even small negative values around 12:00 LT.~~ Micrometeorological parameters such as global radiation ( $R_g$ ) (Zöll et al., 2019), temperature and turbulence (Wolff et al., 2010), humidity (Wyers and Erisman, 1998; Milford et al., 2001), dry/wet leaf surfaces (Wyers and Erisman, 1998; Wentworth et al., 2016), and ~~the~~ concentration of  $\Sigma N_r$ , especially changes in the concentration of the ~~sub-components~~ individual nitrogen compounds, (Brümmer et al., 2013; Zöll et al., 2016) were reported to control the deposition of  $\Sigma N_r$ .

420 In order to investigate the influence of  $u_*$  on the  $\Sigma N_r$  exchange, Fig. S7 illustrates the dependency of  $v_d$  on  $u_*$  for deposition and emission fluxes during day and night. The  $R_g$  threshold for day and nighttime fluxes was set to 10  $\text{W m}^{-2}$ . For better visibility, we binned data in 0.1  $\text{m s}^{-1}$  increments of  $u_*$ . Since bins are not equal in size, we added corresponding half-hourly fluxes to the plots. Red dots represent averages of each bin and error bars correspond to their standard error. We found that  $v_d$  increased slightly with  $u_*$  due to dependency of  $v_d$  on  $R_a$  and  $R_b$ . The latter are proportional to the inverse of  $u_*$  suggesting  
425 that the increase with  $u_*$  should follow a power law. In case of particles, linear relationships between  $u_*$  and  $v_d$  were found by Gallagher et al. (1997); Lavi et al. (2013); Donato and Contini (2014). Although uncertainties of the binned averages were large, a relationship between  $v_d$  and  $u_*$  seems to exist as suggested by the correlations ( $r$ ), but no clear functional relationship could be identified due to the large scattering of half-hourly  $v_d$ .

For visualizing the impact of ~~the~~ concentration on  $v_d$  (Fig. 6), we plotted ~~the~~  $\Sigma N_r$  concentration against the ratio  $v_d/u_*$  in  
430 order to reduce the influence of  $R_a$  and  $R_b$  on  $v_d$ . The threshold for  $R_g$  was set to 10  $\text{W m}^{-2}$ , and we binned data in 0.5  $\mu\text{g N m}^{-3}$  increments of ~~the~~  $\Sigma N_r$  concentration.

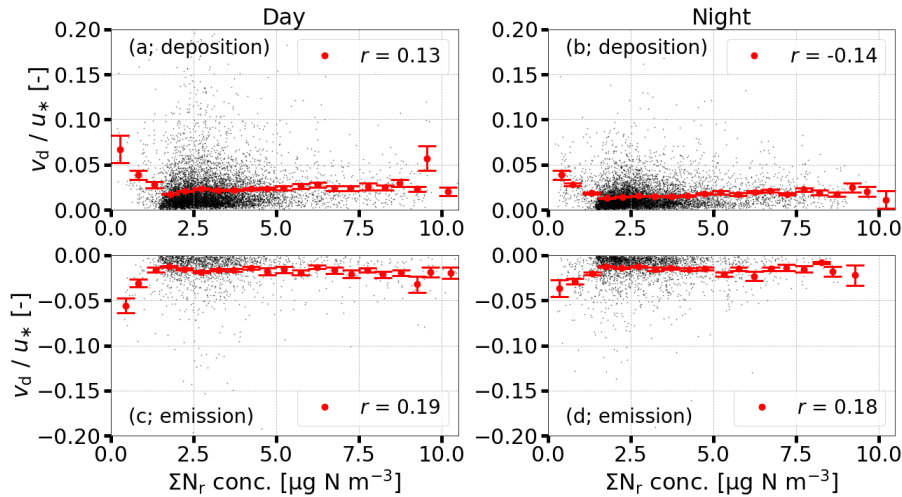


**Figure 6.** Relationships between measured  $\Sigma N_r$  concentrations and corresponding ratios  $v_d/u_*$  separated in emission and deposition during day ((a) and (c)) and night ((b) and (d)). Half-hourly data is displayed in black, red dots represents averages binned in increments of  $0.5 \mu\text{g N m}^{-3}$ . Error bars indicate the standard error of the averages. The threshold for identifying day and nighttime  $v_d$  was set to  $10 \text{ W m}^{-2}$ .  $r$  represents the measure of correlation evaluated for the binned data.

It is obvious that  $v_d/u_*$  exhibited no significant dependence on the  $\Sigma N_r$  concentration as shown by the low values for  $r$ . The ratio appeared to be constant across the (entire) concentration range. It demonstrates that the  $\Sigma N_r$  concentration had no significant influence on their  $v_d$ . In case of particles, the ratio  $v_d/u_*$  depends on Obukov-Length ( $L$ ) and particle size according to Gallagher et al. (1997) and Lavi et al. (2013). In case of deposition fluxes measured during daytime, we found that the ratio decreased for  $-0.2 > L^{-1} < 0$  up to a minimum if  $L^{-1}$  reaches zero (neutral stratification) (Fig. S8). This relationship was observed by Gallagher et al. (1997) and Lavi et al. (2013). Although the scattering of half-hourly ratios is large, the decrease of the ratio with increasing  $L^{-1}$  as well as the dependence of  $v_d$  on  $u_*$  demonstrate that  $v_d$  had a higher affinity to was more influenced by micrometeorological parameters than to variables than by the  $\Sigma N_r$  concentration.

From the analysis of Figs. 6, S7, and S8, it is impossible to state  $u_*$  or  $L$  as the controlling variable of the  $\Sigma N_r$  exchange since turbulence, stratification,  $R_g$ , sensible heat flux, air temperature, and relative humidity are highly correlated with each other. Figure S9 shows the daily diurnal cycle of concentration,  $R_g$ ,  $u_*$ , air temperature ( $T_{\text{air}}$ ), and  $v_d$  for the period from May to September. During that period, a clear diurnal pattern in  $v_d$  was observed with largest values around noon and lowest values during the night. Figure S10 is made for the same variables but for December, January, and February. During winter (December, January, and February) (Fig. S10),  $v_d$  was almost equal and even lower during the day, which resulted in a lower deposition of  $\Sigma N_r$  during winter. The different shapes of the diurnal variations of  $v_d$  could be induced by micrometeorological parameters variables, which change the composition of available  $\Sigma N_r$  compounds during the day (Seinfeld and Pandis, 2006) (e.g., Munger et al., 1996; Horii et al., 2004, 2006; Wyers and Duyzer, 1997; Van Oss et al., 1998) and promote photosynthesis (e.g. stomatal uptake or release of  $\text{NO}_2$  (Thoene et al., 1996) and  $\text{NH}_3$  (Wyers and Erisman, 1998)).

450 Within the period of enhanced  $\Sigma N_r$  exchange, in particular from May to September, we investigated the dependency of the  $\Sigma N_r$  deposition velocities on  $T_{\text{air}}$ , relative humidity ( $RH$ ), dry/wet leaf surface, and  $\Sigma N_r$  concentration. We separated half-hourly  $v_d$  into groups of low and high  $T_{\text{air}}$ ,  $RH$ , and concentration according to their median. In case of separating  $v_d$  into groups of dry and wet leaf surfaces, we used the proposed calculation scheme of a leaf wetness boolean (see Sec. 2.2). No significant influence of the different installation heights on leaf surface wetness was found (see Fig. S11 and corresponding description in the supplement). Figure 7 shows the results for  $v_d$ .

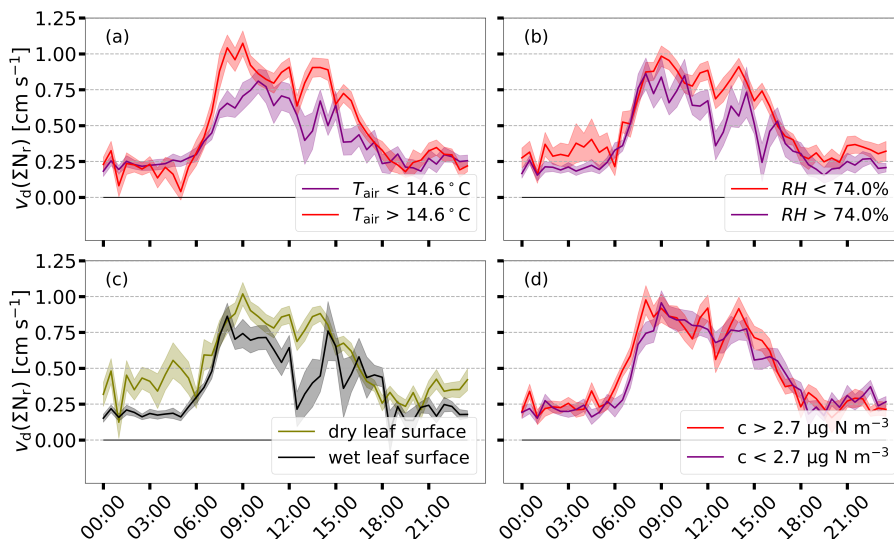


**Figure 7.** Mean daily diurnal cycle of  $v_d$  from May to September of  $v_d$  for low and high temperature (a), relative humidity (b), and concentration (c). Median values of temperature, humidity, and concentration, which are derived for the same time period, are used as threshold values for separating  $v_d$ . In panel (d), the mean daily diurnal cycle of  $v_d$  for dry and wet leaf surfaces is shown. For classifying leaf surfaces as dry or wet, the scheme proposed in Sec. 2.2 is applied. The shaded areas represent the standard error of the mean.

In general, higher air temperatures, less lower relative humidity, and dry leaf surfaces were associated with enhanced deposition of  $\Sigma N_r$ , and a clear diurnal pattern was observed for  $v_d$  with high values around noon and low, non-zero values in the night. During dawn/nighttime, deposition velocities exhibited no significant difference between the applied temperature and humidity thresholds. In the presence of dry leaf surfaces,  $v_d$  was higher by approximately  $0.2 \text{ cm s}^{-1}$  compared to wet leaf surfaces during the night. During the entire day, no difference was found for low and high concentration regimes. During other times of the year, no diurnal pattern was observed. In those periods,  $v_d$  was almost constant and exhibited lower values during daylight compared to the May to September time-frame period. Occasionally, negative deposition velocities referring to emission of  $\Sigma N_r$  were recorded during times of lower radiation.

### 3.4 Sensitivity Dependence of $\Sigma N_r$ dry deposition sums to micrometeorological parameters variables

465 We found that preferentially micrometeorological variables enhance deposition velocities and fluxes. The application of data-driven gap-filling methods like MDV (Falge et al., 2001) for estimating dry deposition could lead to biased results if micrometeorological conditions of the certain gap are different to fluxes used for filling the gap. Therefore, we determined dry deposition budgets with and without  $u_*$ -filter and conducted gap-filling with additional conditions for temperature, relative humidity, and wind speed.

470 Figure 8 shows the non gap-filled  $\Sigma N_r$  fluxes depicted as box plots and their cumulative sums with and without a  $u_*$ -filter if OMDV is used as gap-filling approach. For details to the implementation of OMDV, we refer to see Sec 2.3.

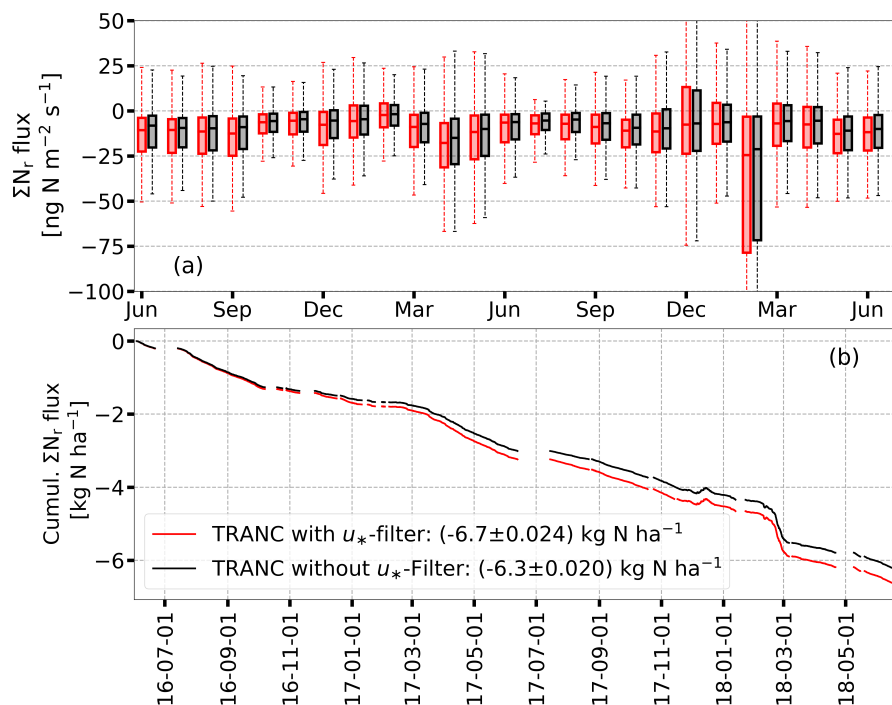


**Figure 8.** Panel (a) shows the non-gap filled  $\Sigma N_r$  fluxes depicted as represented by box-and-whisker plots with (red) and without (black)  $u_*$ -filter in  $\text{ng N m}^{-2} \text{s}^{-1}$  (box frame = 25% to 75% interquartile ranges (IQR), bold line = median, whisker =  $1.5 \cdot \text{IQR}$ ). The threshold for  $u_*$  was set to  $0.1 \text{ m s}^{-1}$ . In panel (b), the cumulative dry deposition of  $\Sigma N_r$  is plotted for both cases in  $\text{kg N ha}^{-1}$ . For determining the cumulative curves, OMDV was used as gap-filling method, and gaps were filled with fluxes being in a range of  $\pm 5$  days. Remaining gaps were not filled. In the legend of panel (b), cumulative  $\Sigma N_r$  deposition and the total uncertainty of the gap-filled fluxes according to Eq. (3) (Pastorello et al., 2020) (see Sec. 4.3) are shown.

The difference in dry deposition was approximately  $400 \text{ g N ha}^{-1}$  after 2 years and corresponds to 6% of the cumulative sum with  $u_*$ -filter. Panel (a) of Fig. 8 shows that median depositions of the  $\Sigma N_r$  fluxes with  $u_*$ -filter were equal to or larger than the median depositions without  $u_*$ -filter. Thus, the applied  $u_*$  threshold removed not only small fluxes resulting

475 in a consistent bias between the median deposition~~s~~. The contribution of the water vapor correction (Eq. 1) to the estimated dry deposition was very low.  $\Sigma N_r$  interference fluxes were between  $-3$  and  $-0.3 \text{ ng N m}^{-2}\text{s}^{-1}$ . The uncertainty ranged between  $0.0$  and  $0.5 \text{ ng N m}^{-2}\text{s}^{-1}$ . Considering two years of TRANC flux measurements with OMDV as gap-filling approach, the correction contributed with  $131 \text{ g ha}^{-1}$  to the estimated dry deposition of  $6.7 \text{ kg ha}^{-1}$ .

480 In order to evaluate the influence of micrometeorological variables such as temperature ( $T$ ),  $RH$ , and wind speed ( $wsp$ ) on annual  $\Sigma N_r$  dry deposition, we compared the deposition estimates of OMDV with CMDV in regard to the measurement years from the beginning of June to end of May (Fig. 9). Details about the implementation of CMDV are given in Sec. 2.3.

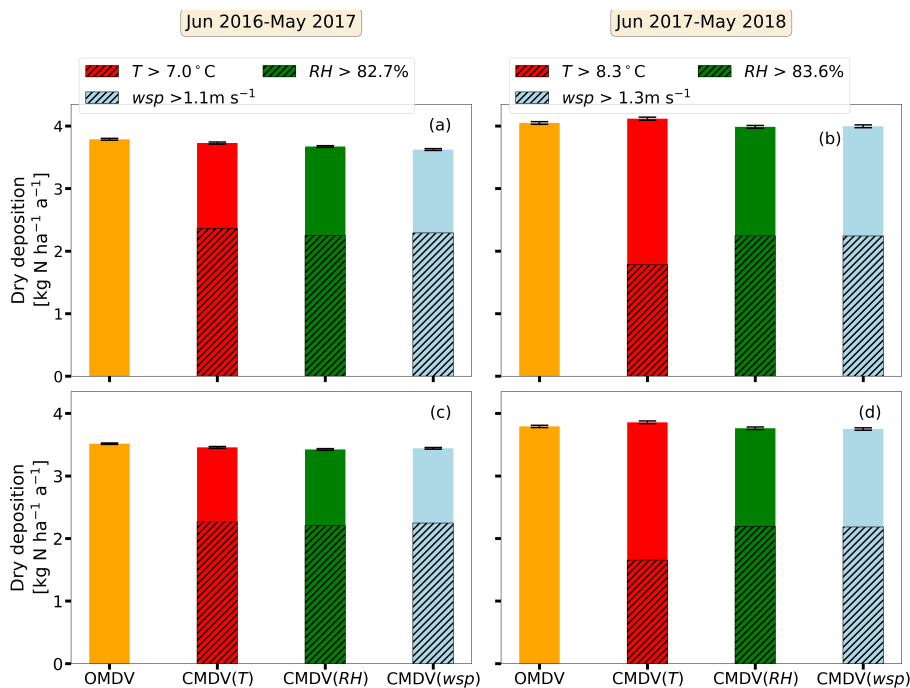


**Figure 9.** Annual  $\Sigma N_r$  dry deposition ~~depicted~~ shown as bar graphs from June to May in  $\text{kg N ha}^{-1} \text{ a}^{-1}$ . For the orange bar, short-term gaps were filled with the OMDV approach while using only fluxes in the time frame of  $\pm 5$  days. In case of the red, green, and blue bar, the CMDV approach is applied for temperature ( $T$ ), relative humidity ( $RH$ ), and wind speed ( $wsp$ ). Fluxes used for CMDV have to additionally be in a range for  $T$  ( $\pm 3^\circ\text{C}$ ),  $RH$  ( $\pm 5\%$ ), or  $wsp$  ( $\pm 1.5 \text{ ms}^{-1}$ ). For OMDV and CMDV, remaining gaps were replaced by monthly averages estimated for each half-hour calculated from the non-gap-filled fluxes. (a) and (b) were made for fluxes with  $u_*$ -filter, (c) and (d) without it. The hatched area of the bars represent the dry deposition for  $T$ ,  $RH$ , and  $wsp$  values higher than the annual median shown in the legend. Error bars correspond to the total uncertainty of the gap-filled fluxes (see Eq. (3)).

No significant difference could be found between the dry deposition~~s~~ sums and their cumulative uncertainties related to gap-filling for both measurement years. Consequently, the applied selection criteria did not lead to biased sums compared to the dry deposition calculated with OMDV. The relative contribution to dry deposition related to temperatures, relative humidity, and wind speeds above their respective medians was at 60% and at 55% in the first and second measurement year, respectively.

As shown before, a difference in the application of a  $u_*$ -filter exists but is within the uncertainty range. Dry deposition was higher in 2017/2018, which was related to the large deposition fluxes observed in February 2018. Still, differences between the years were within their uncertainty ranges. In total, we estimated  $3.8 \text{ kg N ha}^{-1} \text{ a}^{-1}$  and  $4.0 \text{ kg N ha}^{-1} \text{ a}^{-1}$  with the OMDV approach (orange bar) and  $u_*$ -filter for 2016/2017 and 2017/2018, respectively.

### 490 3.5 Wet and total nitrogen deposition

Wet deposition was estimated from measurements of bulk and wet-only samplers. Table 1 shows estimated  $\Sigma N_r$  dry depositions, the deposition estimates of  $\text{NH}_4^+$ -N,  $\text{NO}_3^-$ -N, dissolved organic nitrogen (DON), and the resulting total nitrogen from wet deposition (TWD) for all seasons and both measurement years. Please note that the sum of all seasons corresponds to the sum of both measurement years.

**Table 1.** Annual and seasonal sums of dry deposition estimates (DD) and  $\text{NH}_4^+$ -N,  $\text{NO}_3^-$ -N, dissolved organic nitrogen (DON), and the resulting total wet deposition (TWD) from wet deposition samplers (bulk (BD) and wet-only (WD)) in  $\text{kg N ha}^{-1} \text{ period}^{-1}$ .

Time	DD [ $\text{kg N ha}^{-1} \text{ period}^{-1}$ ]	WD [ $\text{kg N ha}^{-1} \text{ period}^{-1}$ ]				BD [ $\text{kg N ha}^{-1} \text{ period}^{-1}$ ]			
		$\text{NO}_3^-$ -N	$\text{NH}_4^+$ -N	DON	TWD	$\text{NO}_3^-$ -N	$\text{NH}_4^+$ -N	DON	TWD
Winter	2.0	1.5	0.9	0.4	2.8	1.7	1.3	0.5	3.5
Spring	2.2	1.8	2.3	0.1	4.2	1.9	2.4	0.1	4.4
Summer	2.0	1.9	2.6	0.2	4.7	1.6	2.2	0.6	4.4
Autumn	1.7	1.5	1.4	0.6	3.5	1.4	1.4	0.6	3.4
June 16 – May 17	3.8	3.8	4.2	0.4	8.4	3.5	4.2	1.0	8.7
June 17 – May 18	4.0	2.9	3.1	0.9	6.9	3.0	3.1	0.9	7.0

495 Small seasonal and annual differences in dry deposition were determined (approx.  $200 \text{ g N ha}^{-1} \text{ period}^{-1}$ ). Total seasonal and annual uncertainties related to gap-filling (Eq. (3)) were between 7 and  $21 \text{ g N ha}^{-1} \text{ period}^{-1}$ . Dry deposition contributed approximately one third to total deposition except for winter (Fig. S12). In the second year, the contribution of dry deposition was higher than in the first year. Higher fractions of dry deposition were related to the large dry deposition occurring in late February 2018. Thus, dry deposition and its uncertainty were remarkably high during winter. Total wet deposition (TWD) was  
500 highest in spring and summer (Figs. 2 and S2). During those periods,  $\text{NH}_4^+$ -N contributed most to TWD, which was probably related to high  $\text{NH}_3$  concentrations. Interseasonal differences for  $\text{NO}_3^-$ -N were found but were lower compared to changes in  $\text{NH}_4^+$ -N. DON deposition was lowest and was between  $0.1$  and  $0.6 \text{ kg N ha}^{-1} \text{ a}^{-1}$ . Overall, differences in TWD for both sampler types were less than  $300 \text{ g N ha}^{-1} \text{ a}^{-1}$  except for winter. Total wet + dry deposition was equivalent to  $12.2 \text{ kg N ha}^{-1} \text{ a}^{-1}$  for 2016/2017 and  $10.9 \text{ kg N ha}^{-1} \text{ a}^{-1}$  for 2017/2018.

#### 4.1 Interpretation of measured concentrations and fluxes

Measured half-hourly  $\Sigma N_r$  concentrations were low relative to sites exposed to agricultural activities or urban environments. On average, we measured 5.5 ppb ( $3.1 \mu\text{g N m}^{-3}$ )  $\Sigma N_r$ , 1.8 ppb ( $1.0 \mu\text{g N m}^{-3}$ )  $\text{NH}_3$ , and 2.5 ppb ( $1.4 \mu\text{g N m}^{-3}$ )  $\text{NO}_x$ . Wintjen et al. (2020) determined an average  $\Sigma N_r$  concentration level of 21 ppb ( $12 \mu\text{g N m}^{-3}$ ) for a seminatural peatland, Brümmer et al. (2013) measured between 7 and 23 ppb (4 and  $13 \mu\text{g N m}^{-3}$ ) as monthly averages above a cropland site, and Ammann et al. (2012) measured half-hourly  $\Sigma N_r$  concentrations ranging from less than 1 ppb to 350 ppb ( $0.6$  to  $201 \mu\text{g N m}^{-3}$ ) for a grassland site. Only for certain time periods,  $\Sigma N_r$  concentrations reached significantly higher values. During winter,  $\text{NO}_x$  increased due to emission from heating with fossil fuels and from combustion processes, for example through traffic and power plants. A generally lower mixing height, which is often observed during winter, also leads to higher ground-level concentrations of air pollutants. In spring and autumn, higher  $\Sigma N_r$  concentrations can be attributed to  $\text{NH}_3$  emission from the application of fertilizer and livestock farming in the surrounding environment (Beudert and Breit, 2010).  $\text{NH}_3$  emissions from livestock farming in rural districts around the NPBW are approximately half of the emissions compared to rural districts located in the Danube-Inn valley (Beudert and Breit, 2010). The authors measured concentrations of  $\text{NO}_2$  (2.1-4.8 ppb ( $1.2$ - $2.8 \mu\text{g N m}^{-3}$ )),  $\text{NO}$  (0.4-1.6 ppb ( $0.2$ - $0.9 \mu\text{g N m}^{-3}$ )) and  $\text{NH}_3$  (1.4 ppb ( $0.8 \mu\text{g N m}^{-3}$ )) at the same site. Those values for  $\text{NO}_2$  and  $\text{NO}$  refer to 1992 until the end of 2008,  $\text{NH}_3$  was measured from mid of 2003 to 2005. The low concentration level and seasonal variability of the  $\Sigma N_r$  compounds, in particular  $\text{NH}_3$  and  $\text{NO}_2$ , are in agreement with Beudert and Breit (2010). Low concentration values of  $\text{NH}_3$  and  $\text{NO}_x$  are reasonable for a site, which is some kilometers away from anthropogenic emission sources. Studies like Wyers and Erisman (1998); Horii et al. (2004); Wolff et al. (2010) conducted measurements of  $\text{NH}_3$  and  $\text{NO}_2$  above remote (mixed) forests and reported similar concentrations for those gases.

Our measurements further indicated that  $\text{NO}_x$  made the highest contribution to the measured  $\Sigma N_r$  concentrations. At the measurement height, the contribution of  $\text{NO}$  to  $\text{NO}_x$  was negligible. Median contribution of  $\text{NO}$  to  $\text{NO}_x$  concentrations was approximately 10% at 50 m.  $\text{NO}$  exhibits higher concentrations and fluxes close to the forest floor as shown by Rummel et al. (2002). Even if soil  $\text{NO}$  was converted to  $\text{NO}_2$  it could still contribute to the measured  $\Sigma N_r$  flux except for the fraction that is removed by the canopy. As mentioned in Sec. 2.2,  $\text{NO}_2$  concentrations had been measured at 50 m. Seok et al. (2013) reported marginal differences in  $\text{NO}_2$  concentrations above the canopy at a remote site. Above the canopy, height differences in  $\text{NO}_2$  concentrations were probably not relevant for the measurement site. The  $\text{NO}_x$  analyzer was equipped with a thermal converter and likely cross-sensitive to other  $\text{NO}_y$  compounds. However, measured concentrations of  $\text{HNO}_3$  or  $\text{NO}_3^-$  were comparatively low as seen in Fig. 2. Thus, their influence on  $\text{NO}_x$  measurements ~~appeared to be~~ was most likely small. In the context of height differences, we found no systematic difference between  $\text{NH}_3$  concentrations within the canopy and just above the canopy. Only for short time periods, for example in summer 2016 and 2017, differences in passive samplers were found indicating a small  $\text{NH}_3$  flux. Considering the LOD of IVL passive samplers for  $\text{NH}_3$  of  $0.4 \mu\text{g N m}^{-3}$  determined by Dämmgen et al. (2010), shows that passive sampler measurements were conducted close to their LOD. It suggests that the uncertainty of the passive samplers was too large to resolve flux gradients. Still,  $\text{NH}_3$  had a strong presence in the  $\Sigma N_r$  concentration within

the growing period of the plants, in particular during spring and summer. DELTA measurements further suggested that gaseous  $N_r$  influenced the  $\Sigma N_r$  concentration pattern at most was mainly influenced by gaseous  $N_r$ .

The increase in the relative contributions of  $HNO_3$  from spring to summer compared to the decrease of  $NH_4^+$  and  $NO_3^-$  (Fig. 3) can be related to the evaporation of  $NH_4NO_3$  (Wyers and Duyzer, 1997; Van Oss et al., 1998; Schaap et al., 2002). However, the findings of Tang et al. (2015) and Tang et al. (2021) revealed that  $HNO_3$  concentrations measured by the DELTA system using carbonate coated denuders may be significantly overestimated (45% on average) since HONO sticks also at those prepared surfaces. Thus, the measured  $HNO_3$  concentrations should be seen as an upper estimate. Due to the reaction of  $NH_3$  with  $HNO_3$  and sulphuric acid particulate  $NH_4^+$  is formed, available as  $NH_4NO_3$  or  $(NH_4)_2SO_4$  or  $NH_4NO_3$  (Trebs et al., 2005).

These aerosols are mainly in the fine mode and assigned associated with aerodynamic diameters less than  $2.5 \mu m$  ( $PM_{2.5}$ ) (Kundu et al., 2010; Putaud et al., 2010; Schwarz et al., 2016). Since the DELTA cut-off size is approximately  $4.5 \mu m$  (Tang et al., 2015), fine accumulated particles could be adequately detected. Coarse mode  $NO_3^-$  aerosols like sodium nitrate ( $NaNO_3$ ) are formed in the presence of sea salt ( $Na^+$  and  $Cl^-$ ) or other geological minerals or biological particles like pollen (Lee et al., 2008; Putaud et al., 2010). Generally, concentrations of  $Na^+$ ,  $Ca^{2+}$ , and  $Mg^{2+}$  were close to zero during the entire campaign. On average, we measured  $0.08 \mu g m^{-3}$  for  $Na^+$  and  $0.01 \mu g m^{-3}$  for  $Ca^{2+}$  and  $Mg^{2+}$ . Although these concentrations were close to and lower than the LOD of DELTA (Tang et al., 2021) and partly underestimated by the filters of the DELTA system due to the cut-off size of approximately  $4.5 \mu m$ , it illustrates that coarse mode nitrate levels are not expected to be significant at the measurement site. As noted in Sec. 2.2, cellulose filters were used for collecting  $NO_3^-$  and  $SO_4^{2-}$ . According to Tang et al. (2015), cellulose filters underestimate  $NO_3^-$  and  $SO_4^{2-}$  ions, sulphate by 11% and nitrate by 37%. However, Schaap et al. (2004) found that cellulose filter are appropriate for capturing  $NO_3^-$ . Inside of the TRANC, high temperatures ( $\geq 870^\circ C$ ) probably led to a chemical decomposition of coarse aerosols (Yuvaraj et al., 2003). Marx et al. (2012) found that the TRANC is able to convert  $NaNO_3$ . Thus, we assume that the TRANC's cut-off size was higher resulting in a higher sensitivity to aerosols in the coarse mode. Still, we observed a clear excess of  $NH_4^+$  over  $NO_3^-$ . Presumably, the contribution of  $NO_3^-$  aerosols to TRANC measurements was not significant. In addition, higher oxidized compounds like  $N_2O_5$  or peroxy acetyl nitrates could not be collected by DELTA, but were probably converted by the TRANC. Issues in the temperature stability or CO supply leading to instabilities in the conversion efficiency of the TRANC may be responsible for disagreements to the collection efficiency of the denuders. A key uncertainty was the data coverage of the TRANC, which was 78% on average during the exposure periods. In total, the comparison of the total N concentrations shows that the TRANC can adequately measure  $\Sigma N_r$  concentration.

In general, a comparison of  $\Sigma N_r$  concentrations and fluxes to other studies is difficult due to the measurement of the total nitrogen. Most studies, which have been published so far, focused only on a single or a few compounds of  $\Sigma N_r$  and are limited to selected sites and time periods of a few days or months. Only a few studies had been focusing on  $\Sigma N_r$  flux measurements using the EC method (see Ammann et al., 2012; Brümmer et al., 2013; Zöll et al., 2019; Wintjen et al., 2020). Brümmer et al. (2013) measured  $\Sigma N_r$  exchange above an agricultural land. During unmanaged phases, fluxes were between  $-20 ng N m^{-2} s^{-1}$  and  $20 ng N m^{-2} s^{-1}$ . Apart from management events, fluxes above the arable field site were closer to zero compared to our unmanaged forest site, which is dominated by deposition fluxes and is therefore a larger sink for reactive nitrogen. Ammann



et al. (2012) measured  $\Sigma N_r$  fluxes above a managed grassland. In the growing season, deposition fluxes of  $-40 \text{ ng N m}^{-2} \text{ s}^{-1}$  were measured. The authors reported increased deposition due to weak  $\text{NO}$  emission during that period. Similar to Brümmer et al. (2013), the flux pattern observed by Ammann et al. (2012) is influenced by fertilizer application and thus, varying contributions of  $N_r$  compounds, for instance by bidirectionally exchanged of  $\text{NH}_3$  leading to both periods of net emission and deposition phases of  $\Sigma N_r$ . Despite the low signal-to-noise ratio of emission fluxes and data coverage of 50% from June 2016 to June 2018 at the measurement site, we were able to investigate the exchange pattern of  $\Sigma N_r$  and could estimate reliable dry deposition sums. To our knowledge, flux measurements of  $\Sigma N_r$  above mixed forests have not been carried out so far. We found that the flux magnitude and diurnal flux pattern were similar to observations reported for individual  $N_r$  species above forests, e.g.  $\text{NH}_3$  (Wyers and Erisman, 1998; Hansen et al., 2013, 2015),  $\text{NO}_2$  (Horii et al., 2004; Geddes and Murphy, 2014),  $\text{HNO}_3$  (Munger et al., 1996; Horii et al., 2006), and total ammonium (tot- $\text{NH}_4^+$ ) and total nitrate (tot- $\text{NO}_3^-$ ) (Wolff et al., 2010). As seen by the flux values and measurements of individual compounds, deposition prevails in the reported flux pattern, which corresponds to our measurements.

However, under certain circumstances regarding micrometeorology or the availability of  $\Sigma N_r$  compounds large deposition or emission fluxes can be observed. In February 2018, remarkably high  $\Sigma N_r$  concentrations and depositions were measured. During the exposure period of the DELTA samplers, we found  $0.96$ ,  $0.17$ ,  $0.37$ ,  $0.27$ , and  $1.70 \text{ } \mu\text{g N m}^{-3}$  for  $\text{NH}_4^+$ ,  $\text{NH}_3$ ,  $\text{NO}_3^-$ ,  $\text{HNO}_3$ , and  $\text{NO}_x$ , respectively. The aerosol concentrations were exceptionally large in February 2018, which have affected these averages considerably. Averaged  $\text{NH}_4^+$  concentration during winter excluding February 2018 was only  $0.38 \text{ } \mu\text{g N m}^{-3}$  in comparison to  $0.96 \text{ } \mu\text{g N m}^{-3}$  for February 2018. The concentration in this month results in a  $\text{NH}_4^+$  concentration 2.5 times higher than the average. Also, the  $\text{SO}_2$  concentration was much larger concentrations ( $1.54 \text{ } \mu\text{g N m}^{-3}$ ) in this month compared to the other winter month ( $0.37 \text{ } \mu\text{g N m}^{-3}$ ). Figure 10 shows the relative contributions of each  $N_r$  compound for February 2018 compared to averaged fractions during winter excluding February 2018.

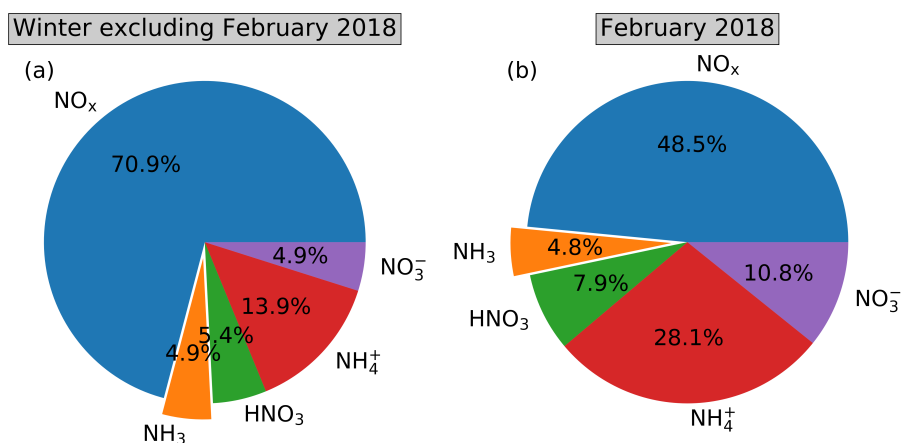


**Figure 10.** Relative contribution of concentrations for  $\text{NO}_x$ ,  $\text{NH}_3$ ,  $\text{HNO}_3$ ,  $\text{NO}_3^-$ , and  $\text{NH}_4^+$  to  $\Sigma N_r$  estimated from DELTA and  $\text{NO}_x$  measurements for winter and separately for February 2018.  $\text{NO}_x$  measurements are averaged to exposure periods of the DELTA samplers.

595 During February 2018,  $\text{NH}_4^+$  made a significant contribution to the  $\Sigma\text{N}_r$  concentration. The measured  $\text{NH}_4^+$  value is an integrated value over approximately one month. Thus, daily contributions of  $\text{NH}_4^+$  could have been even higher. Earlier studies by e.g. Wolff et al. (2010) report events with large aerosol deposition. During their campaign, wind speeds were relatively high. Largest aerosol deposition occurred during dry conditions, e.g. low  $RH$ , no rain, and high visibility. Figure S13 shows micrometeorological parameters, deposition velocities, and gap-filled  $\Sigma\text{N}_r$  fluxes from the 12 February to 6 March. Large deposition  
600 fluxes were accompanied by high  $w_{sp}$  and  $u_*$  values, high  $R_g$  indicating high visibility, and low  $RH$ . The observed conditions are typical for cold air streams with high aerosol loads coming from North east and led to a reduction in turbulent resistances resulting in a high  $v_d$ , which is ~~allowed by turbulence due to efficient turbulent mixing~~. Hence, ~~even~~ at low concentrations of  $\text{NH}_4^+$  significant aerosol deposition is possible if  $R_a$  and the surface resistance are reduced. In conclusion, ~~particulate  $\text{NH}_4^+$  aerosols, ammonium (bi)sulfate and nitrate, were most~~ was mainly responsible for the large  $\Sigma\text{N}_r$  deposition due to ~~their~~ ~~its~~  
605 excess over aerosol  $\text{NO}_3^-$ . Since we had no high-resolution flux measurements of any  $\Sigma\text{N}_r$  compound, we have no evidence which aerosol predominated the  $\Sigma\text{N}_r$  flux.

In December 2017, large emission fluxes were measured. Compared to 2016, significant difference in temperature and snowdepth were observed. Figure 11 shows recorded temperature, snow fall, concentrations, and estimated fluxes of  $\Sigma\text{N}_r$  from 6 December to 15 December for 2016 and 2017. Here,  $\pm 3$  days were chosen for filling the gaps in order to keep the short-term  
610 variability of the fluxes.

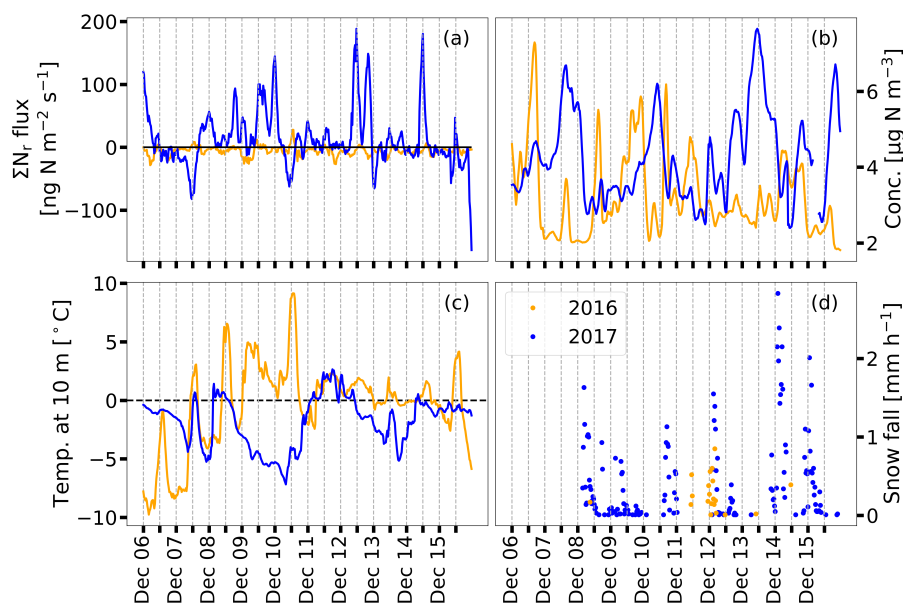


**Figure 11.**  $\Sigma\text{N}_r$  gap-filled fluxes (a),  $\Sigma\text{N}_r$  concentrations (b), air temperature at 10 m height above ground (c), and snow fall (d) from 6 December to 15 December for 2016 (orange) and 2017 (blue). Gaps are filled with the OMDV approach with fluxes being in a range of  $\pm 3$  days. Fluxes and concentrations of  $\Sigma\text{N}_r$  were smoothed with a 3-h-running mean for better visualization.

In 2017, we observed substantial snow fall and a slower varying temperature compared to 2016 leading to significant snow depths compared to 2016. On the 1st of December, 1 cm and 20 cm snow depth were measured in the fetch of the tower for 2016 and 2017, respectively. Two weeks later, snow depth increased to 5 cm and 60 cm, respectively. In addition, temperatures alternated around 0°C with minimum and maximum values close to  $\pm 10^\circ\text{C}$  in December 2016. In 2017, temperatures were  
615 below 0°C and only for one day above 0°C, and global radiation was below  $100 \text{ W m}^{-2}$ .

The decomposition of organic matter, e.g. leaves, litter from the forest ground occurring on the topsoil could be responsible for the observed  $\Sigma\text{N}_r$  emission fluxes of  $\Sigma\text{N}_r$  although the decomposition rate of litter is reduced at lower temperatures. Due to the large snow depth in December 2017, the snow pack could act as an isolator and, inhibited soil frost penetration, and therewith promote decomposition processes. Therefore, decomposition of litter could have been occurring under the snow pack.  
620 ~~Kreyling et al. (2013) compared different snow treatments and their effect on decomposition. The authors observed nearly no soil frost penetration under snow insulation. The annual cellulose decomposition was greatly reduced for the snow removal treatment (~46%). An increasing mass loss rate was found under a deeper snow pack (Saccione et al., 2013) depending on the type and age of litter (Bokhorst et al., 2013). Due to a small snow depth in 2016, soil frost penetration had a higher potential to reduce the decomposition rate. In December 2016, decomposition rates were likely reduced compared to 2017 since snow~~  
625 ~~depth was smaller (e.g. Bokhorst et al., 2013; Kreyling et al., 2013; Saccione et al., 2013). NO seems to be less responsible for the observed emission pattern following the findings of Medinets et al. (2016). They found that NO fluxes were positively correlated to air and soil temperature. Snow cover was not identified as a determining factor for the NO fluxes by the authors, since NO efflux during snow cover and snow free periods were similar. However, the reported snow depth was only 4.6 cm on average. Soil frost penetration could have happened in the topsoil and lowered the NO emissions leading to lower correlation~~  
630 ~~between NO and snow cover. The influence of snow cover on soil emissions of  $\text{N}_r$  compounds, for example NO, is still under discussion (Medinets et al., 2016). As stated by the authors, different results had been published about the origin of NO emissions from snow covered soils (see Medinets et al., 2016, and references therein). An influence of NO either emitted from the snow pack or the soil cannot be fully excluded. A correlation of the measured fluxes with temperature was not found. This could be related to a time-shift between emission and dropping temperature. It has also to be considered that we measure~~  
635 ~~approximately 30 m above the forest soil, and not only NO contributes  $\Sigma\text{N}_r$ . In addition, NO emitted from the forest floor can be converted to  $\text{NO}_2$  (Rummel et al., 2002). Thus, low correlations of  $\Sigma\text{N}_r$  fluxes to micrometeorological parameters were expected. Since we conducted no measurements of NO close to or at the forest floor, we were not able to examine the influence~~  
640 ~~NO emissions from soil or snow on the  $\Sigma\text{N}_r$  measurements. Since soil emitted NO is rapidly converted to  $\text{NO}_2$  (Rummel et al., 2002), the measured  $\Sigma\text{N}_r$  emissions were unlikely to be solely caused by NO. The low correlations of the  $\Sigma\text{N}_r$  fluxes to micrometeorological variables could be related to time-shifts between exchange processes and micrometeorological changes.~~

#### 4.2 Influence of micrometeorology and nitrogen concentrations on deposition and emission

Figure S9 and S10 show that the variability of  $v_d$  and other micrometeorological variables were highly correlated with each other. Thus, we could not examine the mechanistic micrometeorological driver of the  $\Sigma\text{N}_r$  flux. The dependencies on  $u_*$  or  $L$  (Figs. S7 and S8) could also be related to effects of sensible heat flux,  $R_g$  or  $T_{\text{air}}$ . Surely, micrometeorological parameters such

645 as  $R_g$  and  $T_{\text{air}}$  promote photosynthesis of plants (Jarvis, 1976), i.e. lower the stomatal resistance, which is essential for the stomatal uptake of  $\Sigma N_r$  compounds such as  $\text{NO}_2$  (e.g., Thoene et al., 1996) and  $\text{NH}_3$  (e.g., Wyers and Erisman, 1998). Stomatal uptake of  $N_r$  compounds was possible during periods of photosynthetic activity, leading to high values of  $v_d$  during the summer month (Fig. S9). Fig. S10 reveals that a certain degree of  $\Sigma N_r$  uptake still occurred in winter, but deposition decreased strongly during midday, and even periods of emission were observed. These emissions may be due to the decomposition of leaves, 650 leading to a release  $\text{NH}_3$  in late autumn/early winter (Hansen et al., 2013), or from snow-covered soils (see Sec. 4.1).

The analysis of Fig. 6 revealed that deposition velocities were independent of the  $\Sigma N_r$  concentration. ~~Consequently,  $\Sigma N_r$  concentration did not emerge as a driver of its deposition velocities at our measurement site.~~ Still However, the impact of increasing concentrations on nitrogen (deposition) fluxes is well documented, for example, by Ammann et al. (2012) and Brümmer et al. (2013) for  $\Sigma N_r$  above grassland and arable land, respectively, by Horii et al. (2006) for  $\text{NO}_y$  and Horii et al. 655 (2004) for  $\text{NO}_x$  above a mixed forest, and by Zöll et al. (2016) for  $\text{NH}_3$  above a seminatural peatland.

Since we had no possibility to determine the actual contribution of the individual compounds to the  $\Sigma N_r$  flux, comparing micrometeorological dependencies of  $v_d$  to observations made for individual compounds is not possible. In case of  $\text{NH}_3$ , surface wetness was identified as a controlling factor for the  $\text{NH}_3$  uptake in previous studies (Wyers and Erisman, 1998; Milford et al., 2001; Wentworth et al., 2016). For total ammonium and total nitrate (tot- $\text{NH}_4^+$  and tot- $\text{NO}_3^-$ , respectively), 660 Wolff et al. (2010) found that tot- $\text{NO}_3^-$  exchange was ~~almost-neutral~~ nearly zero and emission was observed for tot- $\text{NH}_4^+$  during rain or fog. Highest deposition was observed during sunny days. For the actual compound mix at our measurement site, high temperatures ( $> 14.6^\circ\text{C}$ ), low relative humidity ( $< 74.0\%$ ), and dry leaf surfaces, were found to enhance the surface uptake of  $\Sigma N_r$  from May to September. Since the actual composition of the  $\Sigma N_r$  flux is not known, no arguments about an agreement or disagreement to the cited publications can be made.

665 We further found that the  $\Sigma N_r$  concentration did not change significantly through the year. The difference between lowest and highest seasonal concentration means was only  $0.8 \mu\text{g N m}^{-3}$ . However, DELTA measurements demonstrated that the contribution of individual compounds do show a seasonal cycle. Since the  $\Sigma N_r$  compounds differentiate in their  $v_d$ , the observed seasonality in the dry deposition flux is related to the availability of  $\Sigma N_r$  compounds. For example, in spring and summer,  $\text{NH}_3$  had probably the largest contribution on the  $\Sigma N_r$  flux. Elevated  $\text{NH}_3$  concentrations were likely caused by 670 emissions from agricultural management in the surrounding region (Ge et al., 2020). The concentration of  $\text{NH}_3$  was still lower than of  $\text{NO}_2$ , but the  $v_d$  of  $\text{NH}_3$  is significantly higher than of  $\text{NO}_2$  for woodland. Deposition velocities of  $\text{NH}_3$  range between  $1.1$  and  $2.2 \text{ cm s}^{-1}$  for  $\text{NH}_3$  (see Schrader and Brümmer, 2014, and references therein), and values between  $0.015$  and  $0.51 \text{ cm s}^{-1}$  were reported for  $\text{NO}_2$  (e.g., Rondon et al., 1993; Horii et al., 2004; Breuninger et al., 2013; Delaria et al., 2018, 2020). ~~Still~~ However, variations in the composition of  $\Sigma N_r$  may correlate with micrometeorological parameters. For example, the formation 675 of  $\text{HNO}_3$  is correlated to with  $R_g$ . The solar radiation responsible for the stomatal opening also promotes the formation hydroxyl radicals, which react with  $\text{NO}_x$  to form  $\text{HNO}_3$  (Seinfeld and Pandis, 2006) (e.g., Munger et al., 1996; Horii et al., 2004, 2006; Seinfeld and Pandis, 2006).  $T_{\text{air}}$  influences the diurnal pattern of  $\text{NH}_4\text{NO}_3$ , which may also volatilize close to the surface due to the depletion of its precursors and in a case the temperature gradient is large enough (Wyers and Duyzer, 1997; Van Oss et al., 1998). Thus, some part of the  $\text{NH}_4^+$  and  $\text{NO}_3^-$  in the aerosols phase may be converted to  $\text{NH}_3$  and  $\text{HNO}_3$ ,

680 which can deposit faster to surfaces than aerosols. For  $\text{tot-NH}_4^+$  and  $\text{tot-NO}_3^-$ , mean  $v_d$  of  $3.4 \text{ cm s}^{-1}$  and  $4.2 \text{ cm s}^{-1}$  were determined by Wolff et al. (2010). In case of  $\text{HNO}_3$ , mean values between  $2$  and  $8 \text{ cm s}^{-1}$  were published by Pryor and Klemm (2004); Horii et al. (2006); Farmer and Cohen (2008).

In conclusion, the variability in micrometeorological controls such as  $R_g$ ,  $T_{\text{air}}$ ,  $u_*$ , or  $RH$  in combination with changes in ambient concentration levels of the  $\Sigma N_r$  compounds explain the observed variation in the  $\Sigma N_r$  flux pattern. ~~Definitely,  $\Sigma N_r$  concentration had no influence on its deposition velocities.~~

### 4.3 Uncertainties in dry deposition estimates

Fluxes determined with the EC method are exposed to systematic and random errors. Systematic errors are related to the design of the measurement setup and the instruments, data processing steps including calibration, tilt correction, detrending, and corrections due to low and high-frequency attenuation (Wintjen et al., 2020), and advection fluxes originating preferentially from non-homogeneous surfaces. Uncertainties from the measurement setup were likely caused by an insufficient pump performance, issues in temperature stability of the TRANC and CLD, sensitivity loss of the CLD, and problems in the  $\text{O}_2$  and  $\text{CO}$  supply. Therefore, regular maintenance and continuous observation of instrument performance parameters such as TRANC temperature and flow rate were made. With manual screening of measured half-hourly values and the recording of these parameters, low-quality half-hourly values could be effectively excluded from analysis. A basic assumption for the EC method is that the terrain needs to be flat, and the canopy height and density should be uniform (Burba, 2013). These site criteria are not perfectly fulfilled at our measurement site. The site is located in a low mountain range and tree density is rather sparse south of the flux tower. Such diverse terrain characteristics could lead to unwanted turbulent fluctuations (non-stationarity of time series), which introduce noise in the cross-covariance function. A 2D-footprint analysis exemplarily made for the year 2016 showed that the 70% isoline of the flux had an extension of approximately 300 m. In southwest direction of the tower (approx. distance 100 to 300 m), tree density and height were lower than to the northeast of the tower. Due to the high surface roughness, the flux footprint is limited in its size but the footprint represents the typical forest structure of the NPBW. Thus, we did not filter half-hourly fluxes from certain wind direction sectors.

Random errors are related to turbulence sampling errors (Finkelstein and Sims, 2001; Hollinger and Richardson, 2005; Loescher et al., 2006). An inadequate sample size results in an incomplete sampling of large-scale eddies, which compromises the cross-covariance of the vertical wind and the scalar of interest. The method of Finkelstein and Sims (2001) allows to quantify the random error of the measured fluxes ( $F_{\text{unc, meas}}$ ). In order to determine the effect of the random flux error on the estimated dry deposition sums, we used the method proposed by Pastorello et al. (2020):

$$F_{\text{unc, cum}_i} = \sqrt{\sum_i^n (F_{\text{unc, meas}_i})^2} \quad (3)$$

Using Eq. (3), we determined an uncertainty of  $9 \text{ g N ha}^{-1} \text{ a}^{-1}$  for 2016/2017 and  $21 \text{ g N ha}^{-1} \text{ a}^{-1}$  for 2017/2018 due to insufficient sampling of turbulent motions. The uncertainty related to  $u_*$  filtering is difficult to quantify since common approaches for estimating  $u_*$  thresholds, i.e. Moving Point Threshold (Reichstein et al., 2005) or Change Point Detection (Barr et al., 2013), are designed for  $\text{CO}_2$ . Applying these threshold detection algorithms to  $N_r$  species is not suggested since their

exchange patterns are characterized by a higher variability for different time scales. The chosen  $u_*$  threshold of  $0.1 \text{ cm s}^{-1}$  should be interpreted as minimal filter to exclude periods of insufficient turbulence (for details see Zöll et al., 2019, Sec. 2.4).  
715 In combination with the MDV approach as gap-filling method, the applied threshold may lead to biased dry deposition sums. As ~~seen shown~~ in Fig. 8, the difference between dry deposition sums was ~~within the error range of the dry deposition sum~~ ~~small compared to estimated dry deposition after 2 years~~. Presumably, not only small fluxes were removed from the analysis by the  $u_*$ -filter. We further showed that the contribution of the water vapor correction was negligible. Brümmer et al. (2013) and Ammann et al. (2012) reported a low contribution of the correction to their observed TRANC fluxes.

720 The uncertainty related to gap-filling of a certain half-hourly value was determined by the standard error of the averaged flux, and their annual and seasonal uncertainties were determined by Eq. (3). Both random errors, the random uncertainty of Finkelstein and Sims (2001) and the uncertainty due to the MDV approach, are negligible. Presumably, systematic errors affected the TRANC measurements at most. However, estimating a total systematic uncertainty is not possible since the contribution of individual systematic errors is not known and their quantification is difficult.

725 Regarding the gap-filling technique, we showed that the results when applying the MDV method were independent of the applied micrometeorological criteria. The differences in  $v_d$  to micrometeorology were observed for a limited time period of the year. During other months, we found no influence of micrometeorological variables such as temperature, humidity, and wet/dry leaf surfaces on diurnal pattern of the  $\Sigma N_r$  fluxes. Thus, the dry deposition sums exhibited no significant differences for the applied micrometeorological criteria. The difference ~~between the estimated in the annual~~ dry depositions ~~for the measurements~~  
730 ~~estimates~~ was likely related to the large deposition occurring in February 2018.

Using the MDV approach is recommended for gaps spanning over not more than a few days. Using statistical gap-filling approaches such as look-up tables, non-linear regression, or MDV (Falge et al., 2001) for longer gaps, is not suggested. Statistical methods like MDV assume a periodic variability with high auto-correlation of fluxes. This assumption is valid for  $\text{CO}_2$ , which has a distinctive ~~daily diurnal~~ cycle. Reactive gases do not exhibit a clearly predictable flux pattern. Their  
735 flux variability depends on micrometeorological conditions and their chemical and physical properties sometimes leading to instationarities in data time series. Gap-filling methods based on inferential modeling or artificial neural networks may be a further valuable option, especially for long-term gaps - if models would be available. Monthly averages estimated for each half-hour do not account for short-term deposition or emission events. Since 80% of measured half-hourly fluxes were deposition fluxes at the measurement site, the applied gap-filling method for long-term gaps is somewhat justified.

740 The results of wet deposition have shown that dry deposition contributes approximately one third to the total deposition, which is comparable to previous nitrogen deposition estimates obtained by canopy budget models at the same site (Beudert and Breit, 2014). ~~The comparison of TRANC measurements with nitrogen throughfall measurements will be shown the second part of this study~~. As shown in Table 1, differences between bulk and wet-only deposition were negligible. Small differences between TWD from wet-only and bulk measurements were related to the sedimentation of inorganic and organic dust particles  
745 or to dry deposition of  $\text{NH}_3$  and  $\text{HNO}_3$  (Staelens et al., 2005). The effects were not relevant for the annual nitrogen deposition at the measurement site. Estimated total N depositions ~~were was~~ in the range of critical loads for *Picea abies* and *Fagus sylvatica* reaching from  $10$  to  $15 \text{ kg N ha}^{-1} \text{ a}^{-1}$  and  $10$  to  $20 \text{ kg N ha}^{-1} \text{ a}^{-1}$ , respectively (Bobbink and Hettelingh, 2011). Since the

forest stand consists to approximately 80% of Norway spruce in the footprint and the surrounding forest stand is predominated by Norway spruce, the critical load for the forest stand is probably closer to the values of *Picea abies*. It suggests that the forest  
750 ~~is currently not in a critical state in relation atmospheric N input.~~ is currently close to the limit of receiving too much nitrogen from the atmosphere assuming that the critical load of the forest site is at the upper end of the reported ranges.

## 5 Conclusions

Our study is the first one presenting 2.5 years of flux measurements of total reactive atmospheric nitrogen ( $\Sigma N_r$ ) measured with a custom-built converter called Total Reative Atmospheric nitrogen converter (TRANC) coupled to fast-response chemi-  
755 luminescence detector (CLD) above a protected ~~temperate~~ mixed forest, ~~that is located in a remote area.~~

A comparison of monthly averaged  $\Sigma N_r$  concentrations from the TRANC and DELTA (DEnuder for Long-Term Atmospheric sampling) and chemiluminescence measurements of nitric oxide (NO) and nitrogen dioxide (NO<sub>2</sub>) showed a reasonable agreement in their seasonal patterns. On average, concentrations by the TRANC-CLD system were higher by  $\sim 0.41 \mu\text{g N m}^{-3}$  showing that the TRANC-CLD system can adequately measure  $\Sigma N_r$  concentrations. Differences could be related to  
760 higher oxidized nitrogen compounds, which are not detected by the DELTA system, an insufficient data coverage of TRANC measurements during the exposure periods, the presumably lower aerosol cut-off size of DELTA, issues in the conversion efficiency of the TRANC, etc.. Only nitrogen oxides (NO<sub>x</sub>) and ammonia (NH<sub>3</sub>) showed distinct seasonal changes in their concentrations whereas  $\Sigma N_r$  concentration remained stable throughout the year. NO<sub>x</sub> exhibited highest concentrations during winter, NH<sub>3</sub> during spring and summer. In total, the sum of both gases had a mean contribution of 71.0% to the  $\Sigma N_r$   
765 concentrations highlighting their importance for the observed  $\Sigma N_r$  exchange pattern.

During 2.5 years of flux measurements, median deposition ranged from -15 to -5 ng N m<sup>-2</sup> s<sup>-1</sup>. Deposition velocities followed the diurnal pattern of the fluxes, and median values ranged between 0.2 and 0.5 cm s<sup>-1</sup>. Highest deposition was observed during ~~the timeframe periods~~ of high ~~incident solar~~ radiation, in particular from May to September. Our findings suggest that seasonal changes in the ~~concentrations contributions~~ of the ~~individually measured~~  $\Sigma N_r$  compounds, global radiation ( $R_g$ ), and  
770 micrometeorological controls correlated with  $R_g$  were most likely responsible for the observed pattern of ~~the deposition velocity~~ ( $v_d$ ). From May to September, ~~deposition-velocity~~ ( $v_d$ ) was elevated in presence of dry leaf surfaces, at a low humidity level, and at higher temperatures. No relationship between  $\Sigma N_r$  concentration and corresponding deposition velocities was found. These findings are exclusively related to the composition of the  $\Sigma N_r$  flux at the measurement site. Comparing results to other sites is challenging due to a different mixture of compounds in the  $\Sigma N_r$  flux. ~~Still, a comparison of measured and modeled  
775 deposition velocities of  $\Sigma N_r$  with the latter being determined by inferential modeling with regard to micrometeorological controls, could hint on deficits in deposition modeling.~~

From June 2016 to May 2017 and June 2017 to May 2018, we estimated dry deposition sums of 3.8 and 4.0 kg N ha<sup>-1</sup> a<sup>-1</sup>, respectively. No significant influence of micrometeorological parameters on ~~estimated dry depositions sums~~  $\Sigma N_r$  fluxes  
780 when using the Mean-Diurnal-Variation approach for filling short-term gaps (up to five days) was found. ~~Remaining half-hourly gaps were replaced by monthly averages of the specific half-hour.~~ ~~Using gap-filling approaches based on inferential~~

~~modeling for long-term gaps, is an option which we investigate in the companion paper.~~ In the first and second measurement year, we determined 12.2 and 10.9 kg N ha<sup>-1</sup> a<sup>-1</sup> as total nitrogen deposition, respectively. Thus, dry deposition contributed approximately 1/3 to the total N deposition. A review of published critical loads show that estimated total deposition were at the lower upper end of the critical load range.

785 The data set presented in this study provides a unique opportunity for a comparison to deposition models. In the second part of this paper, a comparison of the acquired dataset to the performance of deposition models will be made. Modeled exchange dynamics will be discussed in regard to their biophysical controlling factors. Annual N budgets from measurements, modeling approaches using in-situ and modeled input parameters, and canopy outflow measurements will be shown.

*Code and data availability.* All data are available upon request from the first author of this study (pascal.wintjen@thuenen.de). Also, Python 3.7 code for flux data analysis can be requested from the first author.

*Author contributions.* PW, FS, and CB conceived the study. PW wrote the manuscript, carried out the measurements at the forest site, and conducted flux data analysis and interpretation. FS evaluated meteorological measurements. FS and MS provided insights in interpreting deposition velocities. BB performed the wet deposition analysis. CB installed the flux tower equipment and gave scientific advice to the overall data analysis and interpretation. All authors discussed the results and FS, MS, BB, and CB contributed to the manuscript.

795 *Competing interests.* The authors declare that they have no conflict of interest.

*Acknowledgements.* Funding by the German Environment Agency (UBA) (project FORESTFLUX, support code FKZ 3715512110) and by the German Federal Ministry of Education and Research (BMBF) within the framework of the Junior Research Group NITROSPHERE (support code FKZ 01LN1308A) is greatly acknowledged. We thank Undine Zöll for scientific and logistical help, Jeremy Rüffer and Jean-Pierre Delorme for excellent technical support, Ute Tambor, Andrea Niemeyer, and Dr. Daniel Ziehe for conducting laboratory analyses of denuder and filter samples, and the Bavarian Forest Nationalpark (NPBW) Administration, namely Wilhelm Breit and Ludwig Höcker for technical and logistical support at the measurement site. We further thank the anonymous reviewers and the editor for their valuable comments that helped improve the quality of the manuscript significantly.



## References

- 805 Ammann, C., Wolff, V., Marx, O., Brümmner, C., and Neftel, A.: Measuring the biosphere-atmosphere exchange of total reactive nitrogen by eddy covariance, *Biogeosciences*, 9, 4247–4261, <https://doi.org/10.5194/bg-9-4247-2012>, 2012.
- Aubinet, M., Grelle, A., Ibrom, A., Rannik, U., Moncrieff, J., Foken, T., Kowalski, A. S., Martin, P. H., Berbigier, P., Bernhofer, C., Clement, R., Elbers, J., Granier, A., Grünwald, T., Morgenstern, K., Pilegaard, K., Rebmann, C., Snijders, W., Valentini, R., and Vesala, T.: Estimates of the Annual Net Carbon and Water Exchange of Forests: The EUROFLUX Methodology, vol. 30 of *Advances in Ecological Research*, pp. 113–175, Academic Press, [https://doi.org/10.1016/S0065-2504\(08\)60018-5](https://doi.org/10.1016/S0065-2504(08)60018-5), 1999.
- 810 Aubinet, M., Vesala, T., and Papale, D., eds.: *Eddy Covariance: A Practical Guide to Measurement and Data Analysis*, Springer Science+Business Media B.V. 2012, Dordrecht, The Netherlands, 2012.
- Baldocchi, D., Falge, E., Gu, L., Olson, R., Hollinger, D., Running, S., Anthoni, P., Bernhofer, C., Davis, K., Evans, R., Fuentes, J., Goldstein, A., Katul, G., Law, B., Lee, X., Malhi, Y., Meyers, T., Munger, W., Oechel, W., Paw, K. T., Pilegaard, K., Schmid, H. P., Valentini, R., Verma, S., Vesala, T., Wilson, K., and Wofsy, S.: FLUXNET: A New Tool to Study the Temporal and Spatial Variability of Ecosystem-Scale Carbon Dioxide, Water Vapor, and Energy Flux Densities, *Bulletin of the American Meteorological Society*, 82, 2415–2434, [https://doi.org/10.1175/1520-0477\(2001\)082<2415:Fantts>2.3.Co;2](https://doi.org/10.1175/1520-0477(2001)082<2415:Fantts>2.3.Co;2), 2001.
- 815 Baldocchi, D. D.: Assessing the eddy covariance technique for evaluating carbon dioxide exchange rates of ecosystems: past, present and future, *Global Change Biology*, 9, 479–492, <https://doi.org/10.1046/j.1365-2486.2003.00629.x>, 2003.
- Barr, A., Richardson, A., Hollinger, D., Papale, D., Arain, M., Black, T., Bohrer, G., Dragoni, D., Fischer, M., Gu, L., Law, B., Margolis, H., McCaughey, J., Munger, J., Oechel, W., and Schaeffer, K.: Use of change-point detection for friction-velocity threshold evaluation in eddy-covariance studies, *Agricultural and Forest Meteorology*, 171–172, 31–45, <https://doi.org/10.1016/j.agrformet.2012.11.023>, 2013.
- 820 Beudert, B. and Breit, W.: *Integrated Monitoring Programm an der Meßstelle Forellenbach im Nationalpark Bayerischer Wald, Untersuchungen zum Stickstoffeintrag und zum wassergebundenen Stickstoffhaushalt des Forellenbachgebiets*, Förderkennzeichen 351 01 012. Nationalparkverwaltung Bayerischer Wald, Sachgebiet IV, technical report, Umweltbundesamt, Dessau-Roßlau, Germany, [http://www.umweltbundesamt.de/sites/default/files/medien/370/dokumente/ece\\_im\\_forellenbach\\_berichtsjahr\\_2009.pdf](http://www.umweltbundesamt.de/sites/default/files/medien/370/dokumente/ece_im_forellenbach_berichtsjahr_2009.pdf), last access: 8 December 2021, 2010.
- 825 Beudert, B. and Breit, W.: *Kronenraumbilanzen zur Abschätzung der Stickstoffgesamtdeposition in Waldökosysteme des Nationalparks Bayerischer Wald*, technical report, Umweltbundesamt, Dessau-Roßlau, Germany, [https://www.umweltbundesamt.de/sites/default/files/medien/370/dokumente/kronenraumbilanzen\\_stickstoffgesamtdeposition\\_nationalpark\\_bayerisches\\_wald\\_-\\_berichtsjahr\\_2013\\_im\\_forellenbach.pdf](https://www.umweltbundesamt.de/sites/default/files/medien/370/dokumente/kronenraumbilanzen_stickstoffgesamtdeposition_nationalpark_bayerisches_wald_-_berichtsjahr_2013_im_forellenbach.pdf), last access: 8 December 2021, 2014.
- 830 Beudert, B., Bernsteinová, J., Premier, J., and Bässler, C.: Natural disturbance by bark beetle offsets climate change effects on streamflow in headwater catchments of the Bohemian Forest, *Silva Gabreta*, 24, 21–45, [https://www.npsumava.cz/wp-content/uploads/2019/06/2\\_sg\\_24\\_beudertetal.pdf](https://www.npsumava.cz/wp-content/uploads/2019/06/2_sg_24_beudertetal.pdf), last access: 8 December 2021, 2018.
- Bobbink, R. and Hettelingh, J.-P.: Review and revision of empirical critical loads and dose-response relationships, Tech. Rep. RIVM report 680359002, National Institute for Public Health and the Environment (RIVM), <https://www.rivm.nl/bibliotheek/rapporten/680359002.pdf>, last access: 31 October 8 December 2021, 2011.
- 835 Bokhorst, S., Metcalfe, D. B., and Wardle, D. A.: Reduction in snow depth negatively affects decomposers but impact on decomposition rates is substrate dependent, *Soil Biology and Biochemistry*, 62, 157–164, <https://doi.org/j.soilbio.2013.03.016>, 2013.

- Breuninger, C., Meixner, F. X., and Kesselmeier, J.: Field investigations of nitrogen dioxide (NO<sub>2</sub>) exchange between plants and the atmosphere, *Atmospheric Chemistry and Physics*, 13, 773–790, <https://doi.org/10.5194/acp-13-773-2013>, 2013.
- 840 Brümmer, C., Marx, O., Kutsch, W., Ammann, C., Wolff, V., Flechard, C. R., and Freibauer, A.: Fluxes of total reactive atmospheric nitrogen ( $\Sigma N_r$ ) using eddy covariance above arable land, *Tellus B: Chemical and Physical Meteorology*, 65, 19770, <https://doi.org/10.3402/tellusb.v65i0.19770>, 2013.
- Burba, G.: Eddy Covariance Method for Scientific, Industrial, Agricultural and Regulatory Applications: A Field Book on Measuring Ecosystem Gas Exchange and Areal Emission Rates, LI-COR Biosciences, Lincoln, Nebraska, USA, 2013.
- 845 Civerolo, K. L. and Dickerson, R. R.: Nitric oxide soil emissions from tilled and untilled cornfields, *Agricultural and Forest Meteorology*, 90, 307–311, [https://doi.org/10.1016/S0168-1923\(98\)00056-2](https://doi.org/10.1016/S0168-1923(98)00056-2), 1998.
- Trebs, I., Metzger, S., Meixner, F. X., Helas, G., Hoffer, A., Rudich, Y., Falkovich, A. H., Moura, M. A. L., da Silva Jr., R. S., Artaxo, P., Slanina, J., and Andreae, M. O.: The NH<sub>4</sub><sup>+</sup>-NO<sub>3</sub><sup>-</sup>-Cl<sup>-</sup>-SO<sub>4</sub><sup>2-</sup>-H<sub>2</sub>O aerosol system and its gas phase precursors at a pasture site in the Amazon Basin: How relevant are mineral cations and soluble organic acids?, *Journal of Geophysical Research: Atmospheres*, 110, <https://doi.org/10.1029/2004JD005478>, 2005.
- 850 Dämmgen, U., Thöni, L., Lumpp, R., Gilke, K., Seidler, E., and Bullinger, M.: Feldexperiment zum Methodenvergleich von Ammoniak- und Ammonium-Konzentrationsmessungen in der Umgebungsluft, 2005 bis 2008 in Braunschweig, vol. 337 of *Landbauforschung : Sonderheft*, Johann Heinrich von Thünen-Institut, Braunschweig, [https://www.openagrar.de/receive/timport\\_mods\\_00006160](https://www.openagrar.de/receive/timport_mods_00006160), jahresberichtskategorie: 10-M4;10-3, 2010.
- 855 Delany, A. C., Fitzjarrald, D. R., Lenschow, D. H., Pearson, R., Wendel, G. J., and Woodruff, B.: Direct measurements of nitrogen oxides and ozone fluxes over grassland, *Journal of Atmospheric Chemistry*, 4, 429–444, <https://doi.org/10.1007/BF00053844>, 1986.
- Delaria, E. R., Vieira, M., Cremieux, J., and Cohen, R. C.: Measurements of NO and NO<sub>2</sub> exchange between the atmosphere and *Quercus agrifolia*, *Atmospheric Chemistry and Physics*, 18, 14 161–14 173, <https://doi.org/10.5194/acp-18-14161-2018>, 2018.
- 860 Delaria, E. R., Place, B. K., Liu, A. X., and Cohen, R. C.: Laboratory measurements of stomatal NO<sub>2</sub> deposition to native California trees and the role of forests in the NO<sub>x</sub> cycle, *Atmospheric Chemistry and Physics*, 20, 14 023–14 041, <https://doi.org/10.5194/acp-20-14023-2020>, 2020.
- Donateo, A. and Contini, D.: Correlation of Dry Deposition Velocity and Friction Velocity over Different Surfaces for PM<sub>2.5</sub> and Particle Number Concentrations, *Advances in Meteorology*, 2014, 1–12, <https://doi.org/10.1155/2014/760393>, 2014.
- 865 Erisman, J. W. and Wyers, G. P.: Continuous measurements of surface exchange of SO<sub>2</sub> and NH<sub>3</sub>; Implications for their possible interaction in the deposition process, *Atmospheric Environment. Part A. General Topics*, 27, 1937–1949, [https://doi.org/10.1016/0960-1686\(93\)90266-2](https://doi.org/10.1016/0960-1686(93)90266-2), 1993.
- Erisman, J. W., Mennen, M. G., Fowler, D., Flechard, C. R., Spindler, G., Grüner, A., Duyzer, J. H., Ruigrok, W., and Wyers, G. P.: Towards development of a deposition monitoring network for air pollution in Europe, resreport Report no. 722108015, RIVM, the Netherlands, <https://rivm.openrepository.com/bitstream/handle/10029/10432/722108015.pdf;jsessionid=532211C11FE7D0487F070927B24AE8ED?sequence=1>, last access: ~~31 October~~ 8 December 2021, 1996.
- 870 Erisman, J. W., Galloway, J. N., Seitzinger, S., Bleeker, A., Dise, N. B., Petrescu, A. M., Leach, A. M., and de Vries, W.: Consequences of human modification of the global nitrogen cycle, *Philosophical Transactions of the Royal Society London B: Biological Sciences*, 368, 20130 116, <https://doi.org/10.1098/rstb.2013.0116>, 2013.
- 875 Eugster, W. and Hesterberg, R.: Transfer resistances of NO<sub>2</sub> determined from eddy correlation flux measurements over a litter meadow at a rural site on the swiss plateau, *Atmospheric Environment*, 30, 307–311, [https://doi.org/10.1016/1352-2310\(95\)00418-1](https://doi.org/10.1016/1352-2310(95)00418-1), 1996.

- Falge, E., Baldocchi, D., Olson, R., Anthoni, P., Aubinet, M., Bernhofer, C., Burba, G., Ceulemans, R., Clement, R., Dolman, H., Granier, A., Gross, P., Grünwald, T., Hollinger, D., Jensen, N.-O., Katul, G., Keronen, P., Kowalski, A., Lai, C. T., Law, B. E., Meyers, T., Moncrieff, J., Moors, E., Munger, J., Pilegaard, K., Üllar Rannik, Rebmann, C., Suyker, A., Tenhunen, J., Tu, K., Verma, S., Vesala, T., Wilson, K., and Wofsy, S.: Gap filling strategies for defensible annual sums of net ecosystem exchange, *Agricultural and Forest Meteorology*, 107, 43–69, [https://doi.org/10.1016/S0168-1923\(00\)00225-2](https://doi.org/10.1016/S0168-1923(00)00225-2), 2001.
- 880 Famulari, D., Fowler, D., Hargreaves, K., Milford, C., Nemitz, E., Sutton, M. A., and Weston, K.: Measuring Eddy Covariance Fluxes of Ammonia Using Tunable Diode Laser Absorption Spectroscopy, *Water, Air, & Soil Pollution: Focus*, 4, 151–158, <https://doi.org/10.1007/s11267-004-3025-1>, 2004.
- 885 Farmer, D. K. and Cohen, R. C.: Observations of  $\text{HNO}_3$ ,  $\Sigma \text{AN}$ ,  $\Sigma \text{PN}$  and  $\text{NO}_2$  fluxes: evidence for rapid  $\text{HO}_x$  chemistry within a pine forest canopy, *Atmospheric Chemistry and Physics*, 8, 3899–3917, <https://doi.org/10.5194/acp-8-3899-2008>, 2008.
- Farmer, D. K., Wooldridge, P. J., and Cohen, R. C.: Application of thermal-dissociation laser induced fluorescence (TD-LIF) to measurement of  $\text{HNO}_3$ ,  $\Sigma$  alkyl nitrates,  $\Sigma$  peroxy nitrates, and  $\text{NO}_2$  fluxes using eddy covariance, *Atmospheric Chemistry and Physics*, 6, 3471–3486, <https://doi.org/10.5194/acp-6-3471-2006>, 2006.
- 890 Farmer, D. K., Kimmel, J. R., Phillips, G., Docherty, K. S., Worsnop, D. R., Sueper, D., Nemitz, E., and Jimenez, J. L.: Eddy covariance measurements with high-resolution time-of-flight aerosol mass spectrometry: a new approach to chemically resolved aerosol fluxes, *Atmospheric Measurement Techniques*, 4, 1275–1289, <https://doi.org/10.5194/amt-4-1275-2011>, 2011.
- Ferm, M.: A Sensitive Diffusional Sampler, Report L91-172, Swedish Environmental Research Institute, Gothenburg, 1991.
- Ferrara, R. M., Loubet, B., Di Tommasi, P., Bertolini, T., Magliulo, V., Cellier, P., Eugster, W., and Rana, G.: Eddy covariance measurement of ammonia fluxes: Comparison of high frequency correction methodologies, *Agricultural and Forest Meteorology*, 158-159, 30–42, <https://doi.org/10.1016/j.agrformet.2012.02.001>, 2012.
- 895 Ferrara, R. M., Di Tommasi, P., Famulari, D., and Rana, G.: Limitations of an Eddy-Covariance System in Measuring Low Ammonia Fluxes, *Boundary-Layer Meteorology*, <https://doi.org/10.1007/s10546-021-00612-6>, 2021.
- Finkelstein, P. L. and Sims, P. F.: Sampling error in eddy correlation flux measurements, *Journal of Geophysical Research: Atmospheres*, 106, 3503–3509, <https://doi.org/10.1029/2000JD900731>, 2001.
- 900 Flechard, C. R., Nemitz, E., Smith, R. I., Fowler, D., Vermeulen, A. T., Bleeker, A., Erismann, J. W., Simpson, D., Zhang, L., Tang, Y. S., and Sutton, M. A.: Dry deposition of reactive nitrogen to European ecosystems: a comparison of inferential models across the NitroEurope network, *Atmospheric Chemistry and Physics*, 11, 2703–2728, <https://doi.org/10.5194/acp-11-2703-2011>, 2011.
- Flechard, C. R., Massad, R. S., Loubet, B., Personne, E., Simpson, D., Bash, J. O., Cooter, E. J., Nemitz, E., and Sutton, M. A.: Advances in understanding, models and parameterizations of biosphere-atmosphere ammonia exchange, *Biogeosciences*, 10, 5183–5225, <https://doi.org/10.5194/bg-10-5183-2013>, 2013.
- 905 Flechard, C. R., Ibrom, A., Skiba, U. M., de Vries, W., van Oijen, M., Cameron, D. R., Dise, N. B., Korhonen, J. F. J., Buchmann, N., Legout, A., Simpson, D., Sanz, M. J., Aubinet, M., Loustau, D., Montagnani, L., Neiryneck, J., Janssens, I. A., Pihlatie, M., Kiese, R., Siemens, J., Francez, A.-J., Augustin, J., Varlagin, A., Olejnik, J., Juszczak, R., Aurela, M., Berveiller, D., Chojnicki, B. H., Dämmgen, U., Delpierre, N., Djuricic, V., Drewer, J., Dufrière, E., Eugster, W., Fauvel, Y., Fowler, D., Frumau, A., Granier, A., Gross, P., Hamon, Y., Helfter, C., Hensen, A., Horváth, L., Kitzler, B., Kruijt, B., Kutsch, W. L., Lobo-do Vale, R., Lohila, A., Longdoz, B., Marek, M. V., Matteucci, G., Mitosinkova, M., Moreaux, V., Neftel, A., Ourcival, J.-M., Pilegaard, K., Pita, G., Sanz, F., Schjoerring, J. K., Sebastià, M.-T., Tang, Y. S., Uggerud, H., Urbaniak, M., van Dijk, N., Vesala, T., Vidic, S., Vincke, C., Weidinger, T., Zechmeister-Boltenstern, S., Butterbach-Bahl, K., Nemitz, E., and Sutton, M. A.: Carbon–nitrogen interactions in European forests and semi-natural vegetation

- 915 – Part 1: Fluxes and budgets of carbon, nitrogen and greenhouse gases from ecosystem monitoring and modelling, *Biogeosciences*, 17, 1583–1620, <https://doi.org/10.5194/bg-17-1583-2020>, 2020.
- Gallagher, M., Beswick, K., Duyzer, J., Westrate, H., Choularton, T., and Hummelshøj, P.: Measurements of aerosol fluxes to speulder forest using a micrometeorological technique, *Atmospheric Environment*, 31, 359–373, [https://doi.org/10.1016/S1352-2310\(96\)00057-X](https://doi.org/10.1016/S1352-2310(96)00057-X), 1997.
- Galloway, J. N., Aber, J. D., Erisman, J. W., Seitzinger, S. P., Howarth, R. W., Cowling, E. B., and Cosby, B. J.: The Nitrogen Cascade, *BioScience*, 53, 341–356, [https://doi.org/10.1641/0006-3568\(2003\)053\[0341:TNC\]2.0.CO;2](https://doi.org/10.1641/0006-3568(2003)053[0341:TNC]2.0.CO;2), 2003.
- 920 Garland, J. A.: The Dry Deposition of Sulphur Dioxide to Land and Water Surfaces, *Proceedings of the Royal Society A: Mathematical, Physical and Engineering Sciences*, 354, 245–268, <https://doi.org/10.1098/rspa.1977.0066>, 1977.
- Ge, X., Schaap, M., Kranenburg, R., Segers, A., Reinds, G. J., Kros, H., and de Vries, W.: Modeling atmospheric ammonia using agricultural emissions with improved spatial variability and temporal dynamics, *Atmospheric Chemistry and Physics*, 20, 16 055–16 087, <https://doi.org/10.5194/acp-20-16055-2020>, 2020.
- 925 Geddes, J. A. and Murphy, J. G.: Observations of reactive nitrogen oxide fluxes by eddy covariance above two midlatitude North American mixed hardwood forests, *Atmospheric Chemistry and Physics*, 14, 2939–2957, <https://doi.org/10.5194/acp-14-2939-2014>, 2014.
- Hansen, K., Sorensen, L. L., Hertel, O., Geels, C., Skjoth, C. A., Jensen, B., and Boegh, E.: Ammonia emissions from deciduous forest after leaf fall, *Biogeosciences*, 10, 4577–4589, <https://doi.org/10.5194/bg-10-4577-2013>, 2013.
- 930 Hansen, K., Pryor, S. C., Boegh, E., Hornsby, K. E., Jensen, B., and Sorensen, L. L.: Background concentrations and fluxes of atmospheric ammonia over a deciduous forest, *Agricultural and Forest Meteorology*, 214–215, 380–392, <https://doi.org/10.1016/j.agrformet.2015.09.004>, 2015.
- Heiskanen, J., Brümmer, C., Buchmann, N., Calfapietra, C., Chen, H., Gielen, B., Gkritzalis, T., Hammer, S., Hartman, S., Herbst, M., Janssens, I., Jordan, A., Juurola, E., Karstens, U., Kasurinen, V., Kruijt, B., Lankreijer, H., Levin, I., Linderson, M.-L., Loustau, D., Merbold, L., Lund Myhre, C., Papale, D., Pavelka, M., Pilegaard, K., Ramonet, M., Rebmann, C., Rinne, J., Rivier, L., Saltikoff, E., Sanders, R., Steinbacher, M., Steinhoff, T., Watson, A., Vermeulen, A., Vesala, T., Vítková, G., and Kutsch, W.: The Integrated Carbon Observation System in Europe, *Bulletin of the American Meteorological Society*, pp. 1 – 54, <https://doi.org/10.1175/BAMS-D-19-0364.1>, 2021.
- Högberg, P.: Nitrogen impacts on forest carbon, *Nature*, 447, 781–782, <https://doi.org/10.1038/447781a>, 2007.
- 940 Hollinger, D. Y. and Richardson, A. D.: Uncertainty in eddy covariance measurements and its application to physiological models, *Tree Physiology*, 25, 873–85, <https://www.ncbi.nlm.nih.gov/pubmed/15870055>, 2005.
- Horii, C. V., Munger, J. W., Wofsy, S. C., Zahniser, M., Nelson, D., and McManus, J. B.: Fluxes of nitrogen oxides over a temperate deciduous forest, *Journal of Geophysical Research: Atmospheres*, 109, <https://doi.org/10.1029/2003JD004326>, 2004.
- Horii, C. V., Munger, J. W., Wofsy, S. C., Zahniser, M., Nelson, D., and McManus, J. B.: Atmospheric reactive nitrogen concentration and flux budgets at a Northeastern US forest site, *Agricultural and Forest Meteorology*, 136, 159–174, <https://doi.org/10.1016/j.agrformet.2006.03.005>, 2006.
- 945 Hurkuck, M., Brümmer, C., Mohr, K., Grünhage, L., Flessa, H., and Kutsch, W. L.: Determination of atmospheric nitrogen deposition to a semi-natural peat bog site in an intensively managed agricultural landscape, *Atmospheric Environment*, 97, 296–309, <https://doi.org/10.1016/j.atmosenv.2014.08.034>, 2014.
- 950 Ibrom, A., Dellwick, E., Flyvbjerg, H., Jensen, N. O., and Pilegaard, K.: Strong low-pass filtering effects on water vapour flux measurements with closed-path eddy correlation systems, *Agricultural and Forest Meteorology*, 147, 140–156, <https://doi.org/10.1016/j.agrformet.2007.07.007>, 2007.

- Jarraud, M.: Guide to meteorological instruments and methods of observation (WMO-No. 8), World Meteorological Organization, Geneva, Switzerland, 2008.
- 955 Jarvis, P. G.: The Interpretation of the Variations in Leaf Water Potential and Stomatal Conductance Found in Canopies in the Field, *Philosophical Transactions of the Royal Society B: Biological Sciences*, 273, 593–610, <https://doi.org/10.1098/rstb.1976.0035>, 1976.
- Jensen, N. and Hummelshøj, P.: Derivation of canopy resistance for water vapor fluxes over a spruce forest, using a new technique for the viscous sublayer resistance (correction to vol. 73, p. 339, 1995), *Agricultural and Forest Meteorology*, 85, 289, [https://doi.org/10.1016/S0168-1923\(97\)00024-5](https://doi.org/10.1016/S0168-1923(97)00024-5), 1997.
- 960 Jensen, N. O. and Hummelshøj, P.: Derivation of canopy resistance for water-vapor fluxes over a spruce forest, using a new technique for the viscous sublayer resistance, *Agricultural and Forest Meteorology*, 73, 339–352, [https://doi.org/10.1016/0168-1923\(94\)05083-I](https://doi.org/10.1016/0168-1923(94)05083-I), 1995.
- Kolle, O. and Rebmann, C.: EddySoft Documentation of a Software Package to Acquire and Process Eddy Covariance Data, techreport, MPI-BGC, <https://repository.publisso.de/resource/fri:4414276-1/data>, 2007.
- Kreyling, J., Haei, M., and Laudon, H.: Snow removal reduces annual cellulose decomposition in a riparian boreal forest, *Canadian Journal of Soil Science*, 93, 427 – 433, <https://doi.org/10.1139/CJSS2012-025>, 2013.
- 965 Krupa, S. V.: Effects of atmospheric ammonia (NH<sub>3</sub>) on terrestrial vegetation: a review, *Environmental Pollution*, 124, 179–221, [https://doi.org/10.1016/S0269-7491\(02\)00434-7](https://doi.org/10.1016/S0269-7491(02)00434-7), 2003.
- Kundu, S., Kawamura, K., and Lee, M.: Seasonal variation of the concentrations of nitrogenous species and their nitrogen isotopic ratios in aerosols at Gosan, Jeju Island: Implications for atmospheric processing and source changes of aerosols, *Journal of Geophysical Research: Atmospheres*, 115, <https://doi.org/10.1029/2009JD013323>, 2010.
- 970 Langford, B., Acton, W., Ammann, C., Valach, A., and Nemitz, E.: Eddy-covariance data with low signal-to-noise ratio: time-lag determination, uncertainties and limit of detection, *Atmospheric Measurement Techniques*, 8, 4197–4213, <https://doi.org/10.5194/amt-8-4197-2015>, 2015.
- Lavi, A., Farmer, D., Segre, E., Moise, T., Rotenberg, E., Jimenez, J. L., and Rudich, Y.: Fluxes of Fine Particles Over a Semi-Arid Pine Forest: Possible Effects of a Complex Terrain, *Aerosol Science and Technology*, 47, 906–915, <https://doi.org/10.1080/02786826.2013.800940>, 2013.
- 975 Lee, T., Yu, X.-Y., Ayres, B., Kreidenweis, S. M., Malm, W. C., and Collett, J. L.: Observations of fine and coarse particle nitrate at several rural locations in the United States, *Atmospheric Environment*, 42, 2720–2732, <https://doi.org/10.1016/j.atmosenv.2007.05.016>, vienna Visibility Conference 2006, 2008.
- 980 Lenschow, D. H. and Raupach, M. R.: The attenuation of fluctuations in scalar concentrations through sampling tubes, *Journal of Geophysical Research*, 96, 15 259–15 268, <https://doi.org/10.1029/91JD01437>, 1991.
- Li, Y., Aneja, V. P., Arya, S. P., Rickman, J., Brittig, J., Roelle, P., and Kim, D. S.: Nitric oxide emission from intensively managed agricultural soil in North Carolina, *Journal of Geophysical Research: Atmospheres*, 104, 26 115–26 123, <https://doi.org/10.1029/1999JD900336>, 1997.
- Loescher, H. W., Law, B. E., Mahrt, L., Hollinger, D. Y., Campbell, J., and Wofsy, S. C.: Uncertainties in, and interpretation of, carbon flux estimates using the eddy covariance technique, *Journal of Geophysical Research: Atmospheres*, 111, <https://doi.org/https://doi.org/10.1029/2005JD006932>, 2006.
- LTER: Long Term Ecological Research (LTER) network, <https://deims.org/993ed2fc-1cb0-4810-a619-8bcf78b6ecee>, last access: ~~31 October~~ **8 December** 2021, 2021.
- 990 Magnani, F., Mencuccini, M., Borghetti, M., Berbigier, P., Berninger, F., Delzon, S., Grelle, A., Hari, P., Jarvis, P. G., Kolari, P., Kowalski, A. S., Lankreijer, H., Law, B. E., Lindroth, A., Loustau, D., Manca, G., Moncrieff, J. B., Rayment, M., Tedeschi,

- V., Valentini, R., and Grace, J.: The human footprint in the carbon cycle of temperate and boreal forests, *Nature*, 447, 848–50, <https://doi.org/10.1038/nature05847>, 2007.
- Marx, O., Brümmer, C., Ammann, C., Wolff, V., and Freibauer, A.: TRANC – a novel fast-response converter to measure total reactive atmospheric nitrogen, *Atmospheric Measurement Techniques*, 5, 1045–1057, <https://doi.org/10.5194/amt-5-1045-2012>, 2012.
- 995 Massman, W. J.: The attenuation of concentration fluctuations in turbulent flow through a tube, *Journal of Geophysical Research*, 96, 15 269–15 274, <https://doi.org/10.1029/91JD01514>, 1991.
- Mauder, M. and Foken, T.: Impact of post-field data processing on eddy covariance flux estimates and energy balance closure, *Meteorologische Zeitschrift*, 15, 597–609, <https://doi.org/10.1127/0941-2948/2006/0167>, 2006.
- Medinets, S., Gasche, R., Skiba, U., Schindlbacher, A., Kiese, R., and Butterbach-Bahl, K.: Cold season soil NO fluxes from a temperate forest: drivers and contribution to annual budgets, *Environmental Research Letters*, 11, 114 012, <https://doi.org/10.1088/1748-9326/11/11/114012>, 2016.
- 1000 Milford, C., Hargreaves, K. J., Sutton, M. A., Loubet, B., and Cellier, P.: Fluxes of NH<sub>3</sub> and CO<sub>2</sub> over upland moorland in the vicinity of agricultural land, *Journal of Geophysical Research: Atmospheres*, 106, 24 169–24 181, <https://doi.org/10.1029/2001jd900082>, 2001.
- Min, K.-E., Pusede, S. E., Browne, E. C., LaFranchi, B. W., Wooldridge, P. J., and Cohen, R. C.: Eddy covariance fluxes and vertical concentration gradient measurements of NO and NO<sub>2</sub> over a ponderosa pine ecosystem: observational evidence for within-canopy chemical removal of NO<sub>x</sub>, *Atmospheric Chemistry and Physics*, 14, 5495–5512, <https://doi.org/10.5194/acp-14-5495-2014>, 2014.
- 1005 Moffat, A. M., Papale, D., Reichstein, M., Hollinger, D. Y., Richardson, A. D., Barr, A. G., Beckstein, C., Braswell, B. H., Churkina, G., Desai, A. R., Falge, E., Gove, J. H., Heimann, M., Hui, D. F., Jarvis, A. J., Kattge, J., Noormets, A., and Stauch, V. J.: Comprehensive comparison of gap-filling techniques for eddy covariance net carbon fluxes, *Agricultural and Forest Meteorology*, 147, 209–232, <https://doi.org/10.1016/j.agrformet.2007.08.011>, 2007.
- 1010 Moncrieff, J., Clement, R., Finnigan, J., and Meyers, T.: Averaging, Detrending, and Filtering of Eddy Covariance Time Series, pp. 7–31, Kluwer Academic, Dordrecht, [https://doi.org/10.1007/1-4020-2265-4\\_2](https://doi.org/10.1007/1-4020-2265-4_2), 2004.
- Moncrieff, J. B., Massheder, J. M., deBruin, H., Elbers, J., Friberg, T., Heusinkveld, B., Kabat, P., Scott, S., Soegaard, H., and Verhoef, A.: A system to measure surface fluxes of momentum, sensible heat, water vapour and carbon dioxide, *Journal of Hydrology*, 188, 589–611, [https://doi.org/10.1016/S0022-1694\(96\)03194-0](https://doi.org/10.1016/S0022-1694(96)03194-0), 1997.
- 1015 Moravek, A., Singh, S., Pattey, E., Pelletier, L., and Murphy, J. G.: Measurements and quality control of ammonia eddy covariance fluxes: A new strategy for high frequency attenuation correction, *Atmospheric Measurement Techniques*, 12, 6059–6078, <https://doi.org/10.5194/amt-12-6059-2019>, 2019.
- Munger, J. W., Wofsy, S. C., Bakwin, P. S., Fan, S. M., Goulden, M. L., Daube, B. C., Goldstein, A. H., Moore, K. E., and Fitzjarrald, D. R.: Atmospheric deposition of reactive nitrogen oxides and ozone in a temperate deciduous forest and a subarctic woodland: 1. Measurements and mechanisms, *Journal of Geophysical Research-Atmospheres*, 101, 12 639–12 657, <https://doi.org/10.1029/96JD00230>, 1996.
- 1020 Munger, J. W., Fan, S.-M., Bakwin, P. S., Goulden, M. L., Goldstein, A. H., Colman, A. S., and Wofsy, S. C.: Regional budgets for nitrogen oxides from continental sources: Variations of rates for oxidation and deposition with season and distance from source regions, *Journal of Geophysical Research: Atmospheres*, 103, 8355–8368, <https://doi.org/10.1029/98JD00168>, 1998.
- 1025 Neiryneck, J., Kowalski, A. S., Carrara, A., Genouw, G., Berghmans, P., and Ceulemans, R.: Fluxes of oxidised and reduced nitrogen above a mixed coniferous forest exposed to various nitrogen emission sources, *Environmental Pollution*, 149, 31–43, <https://doi.org/10.1016/j.envpol.2006.12.029>, 2007.

- Nemitz, E., Jimenez, J. L., Huffman, J. A., Ulbrich, I. M., Canagaratna, M. R., Worsnop, D. R., and Guenther, A. B.: An Eddy-Covariance System for the Measurement of Surface/Atmosphere Exchange Fluxes of Submicron Aerosol Chemical Species—First Application Above an Urban Areas, *Aerosol Science and Technology*, 42, 636–657, <https://doi.org/10.1080/02786820802227352>, 2008.
- Pastorello, G., Trotta, C., and Canfora, E. e. a.: The FLUXNET2015 dataset and the ONEFlux processing pipeline for eddy covariance data, *Scientific Data*, 7, 225, <https://doi.org/10.1038/s41597-020-0534-3>, 2020.
- Paulson, C. A.: The Mathematical Representation of Wind Speed and Temperature Profiles in the Unstable Atmospheric Surface Layer, *Journal of Applied Meteorology*, 9, 857–861, [https://doi.org/10.1175/1520-0450\(1970\)009<0857:Tmrows>2.0.Co;2](https://doi.org/10.1175/1520-0450(1970)009<0857:Tmrows>2.0.Co;2), 1970.
- Peake, E. and Legge, A. H.: Evaluation of methods used to collect air quality data at remote and rural sites in Alberta, Canada, in: Proc. 1987 EPA/APCA Symposium on Measurements of Toxic and Related Air Pollutants, APCA, 1987.
- Peake, M.: A Preliminary Report on the Design and Testing of the KAPS (Kananaskis Atmospheric Pollutant Sampler) for the Collection of Acidic and Basic Gases and Fine Particles, Document 0012e/July 8/85. Typskript University Calgary, 1985.
- Pryor, S. and Klemm, O.: Experimentally derived estimates of nitric acid dry deposition velocity and viscous sub-layer resistance at a conifer forest, *Atmospheric Environment*, 38, 2769–2777, <https://doi.org/10.1016/j.atmosenv.2004.02.038>, 2004.
- Putaud, J.-P., Van Dingenen, R., Alastuey, A., Bauer, H., Birmili, W., Cyrys, J., Flentje, H., Fuzzi, S., Gehrig, R., Hansson, H., Harrison, R., Herrmann, H., Hitenberger, R., Hüglin, C., Jones, A., Kasper-Giebl, A., Kiss, G., Kousa, A., Kuhlbusch, T., Löschau, G., Maenhaut, W., Molnar, A., Moreno, T., Pekkanen, J., Perrino, C., Pitz, M., Puxbaum, H., Querol, X., Rodriguez, S., Salma, I., Schwarz, J., Smolik, J., Schneider, J., Spindler, G., ten Brink, H., Tursic, J., Viana, M., Wiedensohler, A., and Raes, F.: A European aerosol phenomenology – 3: Physical and chemical characteristics of particulate matter from 60 rural, urban, and kerbside sites across Europe, *Atmospheric Environment*, 44, 1308–1320, <https://doi.org/10.1016/j.atmosenv.2009.12.011>, 2010.
- Reichstein, M., Falge, E., Baldocchi, D., Papale, D., Aubinet, M., Berbigier, P., Bernhofer, C., Buchmann, N., Gilmanov, T., Granier, A., Grünwald, T., Havránková, K., Ilvesniemi, H., Janous, D., Knohl, A., Laurila, T., Lohila, A., Loustau, D., Matteucci, G., Meyers, T., Miglietta, F., Ourcival, J.-M., Pumpanen, J., Rambal, S., Rotenberg, E., Sanz, M., Tenhunen, J., Seufert, G., Vaccari, F., Vesala, T., Yakir, D., and Valentini, R.: On the separation of net ecosystem exchange into assimilation and ecosystem respiration: review and improved algorithm, *Global Change Biology*, 11, 1424–1439, <https://doi.org/10.1111/j.1365-2486.2005.001002.x>, 2005.
- Rondon, A., Johansson, C., and Granat, L.: Dry Deposition of Nitrogen-Dioxide and Ozone to Coniferous Forests, *Journal of Geophysical Research-Atmospheres*, 98, 5159–5172, <https://doi.org/10.1029/92jd02335>, 1993.
- Rummel, U., Ammann, C., Gut, A., Meixner, F. X., and Andreae, M. O.: Eddy covariance measurements of nitric oxide flux within an Amazonian rain forest, *Journal of Geophysical Research-Atmospheres*, 107, LBA 17–1–LBA 17–9, <https://doi.org/10.1029/2001JD000520>, 2002.
- Saccone, P., Morin, S., Baptist, F., Bonneville, J.-M., Colace, M.-P., Domine, F., Faure, M., Geremia, R., Lochet, J., Poly, F., Lavorel, S., and Clément, J.-C.: The effects of snowpack properties and plant strategies on litter decomposition during winter in subalpine meadows, *Plant and Soil*, 363, 215–229, <https://doi.org/10.1007/s11104-012-1307-3>, 2013.
- Schaap, M., Müller, K., and ten Brink, H.: Constructing the European aerosol nitrate concentration field from quality analysed data, *Atmospheric Environment*, 36, 1323–1335, [https://doi.org/10.1016/S1352-2310\(01\)00556-8](https://doi.org/10.1016/S1352-2310(01)00556-8), 2002.
- Schaap, M., Spindler, G., Schulz, M., Acker, K., Maenhaut, W., Berner, A., Wieprecht, W., Streit, N., Müller, K., Brüggemann, E., Chi, X., Putaud, J.-P., Hitenberger, R., Puxbaum, H., Baltensperger, U., and ten Brink, H.: Artefacts in the sampling of nitrate studied in the “INTERCOMP” campaigns of EUROTRAC-AEROSOL, *Atmospheric Environment*, 38, 6487–6496,

- 1065 <https://doi.org/10.1016/j.atmosenv.2004.08.026>, contains Special Issue section on Measuring the composition of Particulate Matter in the EU, 2004.
- Schrader, F. and Brümmner, C.: Land Use Specific Ammonia Deposition Velocities: a Review of Recent Studies (2004–2013), *Water, Air, and Soil Pollution*, 225, 2114, <https://doi.org/10.1007/s11270-014-2114-7>, 2014.
- Schwarz, J., Cusack, M., Karban, J., Chalupníčková, E., Havránek, V., Smolík, J., and Ždímal, V.: PM<sub>2.5</sub> chemical composition at a rural  
1070 background site in Central Europe, including correlation and air mass back trajectory analysis, *Atmospheric Research*, 176–177, 108–120, <https://doi.org/https://doi.org/10.1016/j.atmosres.2016.02.017>, 2016.
- Seinfeld, J. H. and Pandis, S. N.: *Atmospheric Chemistry and Physics – From Air Pollution to Climate Change*, John Wiley & Sons, New York, USA, 2 edn., 2006.
- Seok, B., Helmig, D., Ganzeveld, L., Williams, M. W., and Vogel, C. S.: Dynamics of nitrogen oxides and ozone above and within a mixed  
1075 hardwood forest in northern Michigan, *Atmospheric Chemistry and Physics*, 13, 7301–7320, <https://doi.org/10.5194/acp-13-7301-2013>, 2013.
- Staelens, J., De Schrijver, A., Van Avermaet, P., Genouw, G., and Verhoest, N.: A comparison of bulk and wet-only deposition at two adjacent sites in Melle (Belgium), *Atmospheric Environment*, 39, 7 – 15, <https://doi.org/https://doi.org/10.1016/j.atmosenv.2004.09.055>, 2005.
- Stella, P., Kortner, M., Ammann, C., Foken, T., Meixner, F. X., and Trebs, I.: Measurements of nitrogen oxides and ozone fluxes by eddy  
1080 covariance at a meadow: evidence for an internal leaf resistance to NO<sub>2</sub>, *Biogeosciences*, 10, 5997–6017, <https://doi.org/10.5194/bg-10-5997-2013>, 2013.
- Sutton, M. A., Tang, Y. S., Miners, B., and Fowler, D.: A New Diffusion Denuder System for Long-Term, Regional Monitoring of Atmospheric Ammonia and Ammonium, *Water, Air and Soil Pollution: Focus*, 1, 145–156, <https://doi.org/10.1023/a:1013138601753>, 2001.
- Sutton, M. A., Simpson, D., Levy, P. E., Smith, R. I., Reis, S., van Oijen, M., and de Vries, W.: Uncertainties in the relationship between  
1085 atmospheric nitrogen deposition and forest carbon sequestration, *Global Change Biology*, 14, 2057–2063, <https://doi.org/10.1111/j.1365-2486.2008.01636.x>, 2008.
- Sutton, M. A., Howard, C. M., Erisman, J. W., Billen, G., Bleeker, A., Grennfelt, P., van Grinsven, H., and Grizzetti, B., eds.: *The European Nitrogen Assessment: sources, effects and policy perspectives*, Cambridge University Press, Cambridge, UK, 2011.
- Sutton, M. A., Reis, S., Riddick, S. N., Dragosits, U., Nemitz, E., Theobald, M. R., Tang, Y. S., Braban, C. F., Vieno, M., Dore, A. J., Mitchell,  
1090 R. F., Wanless, S., Daunt, F., Fowler, D., Blackall, T. D., Milford, C., Flechard, C. R., Loubet, B., Massad, R., Cellier, P., Personne, E., Coheur, P. F., Clarisse, L., Van Damme, M., Ngadi, Y., Clerbaux, C., Skjoth, C. A., Geels, C., Hertel, O., Wichink Kruit, R. J., Pinder, R. W., Bash, J. O., Walker, J. T., Simpson, D., Horvath, L., Misselbrook, T. H., Bleeker, A., Dentener, F., and de Vries, W.: Towards a climate-dependent paradigm of ammonia emission and deposition, *Philosophical Transactions of the Royal Society of London. Series B.: Biological Sciences*, 368, 20130 166, <https://doi.org/10.1098/rstb.2013.0166>, 2013.
- 1095 Tang, Y. S., Simmons, I., van Dijk, N., Di Marco, C., Nemitz, E., Dämmgen, U., Gilke, K., Djuricic, V., Vidic, S., Gliha, Z., Borovecki, D., Mitosinkova, M., Hanssen, J. E., Uggerud, T. H., Sanz, M. J., Sanz, P., Chorda, J. V., Flechard, C. R., Fauvel, Y., Ferm, M., Perrino, C., and Sutton, M. A.: European scale application of atmospheric reactive nitrogen measurements in a low-cost approach to infer dry deposition fluxes, *Agriculture, Ecosystems and Environment*, 133, 183–195, <https://doi.org/10.1016/j.agee.2009.04.027>, 2009.
- Tang, Y. S., Cape, J. N., Braban, C. F., Twigg, M. M., Poskitt, J., Jones, M. R., Rowland, P., Bentley, P., Hockenhull, K., Woods, C., Leaver,  
1100 D., Simmons, I., van Dijk, N., Nemitz, E., and Sutton, M. A.: Development of a new model DELTA sampler and assessment of potential sampling artefacts in the UKEAP AGANet DELTA system: summary and technical report, Tech. rep., London, [https://uk-air.defra.gov.uk/library/reports?report\\_id=861](https://uk-air.defra.gov.uk/library/reports?report_id=861), last access: ~~31 October~~ 8 December 2021, 2015.



- Tang, Y. S., Flechard, C. R., Dämmgen, U., Vidic, S., Djuricic, V., Mitosinkova, M., Uggerud, H. T., Sanz, M. J., Simmons, I., Dragosits, U., Nemitz, E., Twigg, M., van Dijk, N., Fauvel, Y., Sanz, F., Ferm, M., Perrino, C., Catrambone, M., Leaver, D., Braban, C. F., Cape, J. N., Heal, M. R., and Sutton, M. A.: Pan-European rural monitoring network shows dominance of  $\text{NH}_3$  gas and  $\text{NH}_4\text{NO}_3$  aerosol in inorganic atmospheric pollution load, *Atmospheric Chemistry and Physics*, 21, 875–914, <https://doi.org/10.5194/acp-21-875-2021>, 2021.
- 1105 Thoenes, B., Rennenberg, H., and Weber, P.: Absorption of atmospheric  $\text{NO}_2$  by spruce (*Picea abies*) trees, *New Phytologist*, 134, 257–266, <https://doi.org/j.1469-8137.1996.tb04630.x>, 1996.
- UNECE: International Cooperative Program on Integrated Monitoring of Air pollution Effects on Ecosystems (ICP IM) within the framework of the Geneva Convention on Long-Range Transboundary, <http://www.unece.org/env/lrtap/>, last access: ~~31-October~~ 8 December 2021, 2021.
- 1110 Van Oss, R., Duyzer, J., and Wyers, P.: The influence of gas-to-particle conversion on measurements of ammonia exchange over forest, *Atmospheric Environment*, 32, 465 – 471, [https://doi.org/10.1016/S1352-2310\(97\)00280-X](https://doi.org/10.1016/S1352-2310(97)00280-X), 1998.
- van Zanten, M. C., Sauter, F. J., Wichink Kruit, R. J., van Jaarsveld, J. A., and van Pul, W. A. J.: Description of the DEPAC module; Dry deposition modeling with DEPAC\_GCN2010, Tech. rep., RIVM, Bilthoven, NL, 2010.
- 1115 Vickers, D. and Mahrt, L.: Quality Control and Flux Sampling Problems for Tower and Aircraft Data, *Journal of Atmospheric and Oceanic Technology*, 14, 512–526, [https://doi.org/10.1175/1520-0426\(1997\)014<0512:QCAFSP>2.0.CO;2](https://doi.org/10.1175/1520-0426(1997)014<0512:QCAFSP>2.0.CO;2), 1997.
- Webb, E. K.: Profile relationships: The log-linear range, and extension to strong stability, *Quarterly Journal of the Royal Meteorological Society*, 96, 67–90, <https://doi.org/10.1002/qj.49709640708>, 1970.
- 1120 Wentworth, G. R., Murphy, J. G., Benedict, K. B., Bangs, E. J., and Collett Jr, J. L.: The role of dew as a nighttime reservoir and morning source for atmospheric ammonia, *Atmospheric Chemistry and Physics Discussions*, 16, 1–36, <https://doi.org/10.5194/acp-2016-169>, 2016.
- Wesely, M. L.: Parameterization of Surface Resistances to Gaseous Dry Deposition in Regional-Scale Numerical-Models, *Atmospheric Environment*, 23, 1293–1304, [https://doi.org/Doi.10.1016/0004-6981\(89\)90153-4](https://doi.org/Doi.10.1016/0004-6981(89)90153-4), 1989.
- Whitehead, J. D., Twigg, M., Famulari, D., Nemitz, E., Sutton, M. A., Gallagher, M. W., and Fowler, D.: Evaluation of laser absorption spectroscopic techniques for eddy covariance flux measurements of ammonia, *Environ Sci Technol*, 42, 2041–6, <https://doi.org/10.1021/es071596u>, 2008.
- 1125 Wilczak, J. M., Oncley, S. P., and Stage, S. A.: Sonic Anemometer Tilt Correction Algorithms, *Boundary-Layer Meteorology*, 99, 127–150, <https://doi.org/10.1023/A:1018966204465>, 2001.
- Wintjen, P., Ammann, C., Schrader, F., and Brümmner, C.: Correcting high-frequency losses of reactive nitrogen flux measurements, *Atmospheric Measurement Techniques*, 13, 2923–2948, <https://doi.org/10.5194/amt-13-2923-2020>, 2020.
- 1130 Wolff, V., Trebs, I., Foken, T., and Meixner, F. X.: Exchange of reactive nitrogen compounds: concentrations and fluxes of total ammonium and total nitrate above a spruce canopy, *Biogeosciences*, 7, 1729–1744, <https://doi.org/10.5194/bg-7-1729-2010>, 2010.
- Wyers, G. and Duyzer, J.: Micrometeorological measurement of the dry deposition flux of sulphate and nitrate aerosols to coniferous forest, *Atmospheric Environment*, 31, 333 – 343, [https://doi.org/10.1016/S1352-2310\(96\)00188-4](https://doi.org/10.1016/S1352-2310(96)00188-4), 1997.
- 1135 Wyers, G. P. and Erisman, J. W.: Ammonia exchange over coniferous forest, *Atmospheric Environment*, 32, 441–451, [https://doi.org/10.1016/S1352-2310\(97\)00275-6](https://doi.org/10.1016/S1352-2310(97)00275-6), 1998.
- Yuvaraj, S., Fan-Yuan, L., Tsong-Huei, C., and Chuin-Tih, Y.: Thermal Decomposition of Metal Nitrates in Air and Hydrogen Environments, *The Journal of Physical Chemistry B*, 107, 1044–1047, <https://doi.org/10.1021/jp026961c>, 2003.

- 1140 Zöll, U., Brümmner, C., Schrader, F., Ammann, C., Ibrom, A., Flechard, C. R., Nelson, D. D., Zahniser, M., and Kutsch, W. L.: Surface-atmosphere exchange of ammonia over peatland using QCL-based eddy-covariance measurements and inferential modeling, *Atmospheric Chemistry and Physics*, 16, 11 283–11 299, <https://doi.org/10.5194/acp-16-11283-2016>, 2016.
- Zöll, U., Lucas-Moffat, A. M., Wintjen, P., Schrader, F., Beudert, B., and Brümmner, C.: Is the biosphere-atmosphere exchange of total reactive nitrogen above forest driven by the same factors as carbon dioxide? An analysis using artificial neural networks, *Atmospheric Environment*, 206, 108–118, <https://doi.org/10.1016/j.atmosenv.2019.02.042>, 2019.